UNIVERSIDADE DE SÃO PAULO
INSTITUTO DE GEOSCIÊNCIAS

Climate and environmental changes in southwestern Amazon Basin over the last 3000 years based on speleothem isotope records

MARCELA EDUARDA DELLA LIBERA DE GODOY

Orientador: Prof. Dr. Francisco William da Cruz Junior

São Paulo

2021

UNIVERSIDADE DE SÃO PAULO
INSTITUTO DE GEOSCIÊNCIAS

Climate and environmental changes in southwestern Amazon Basin over the last 3000 years based on speleothem isotope records

Marcela Eduarda Della Libera de Godoy

Dissertação de mestrado apresentada ao Programa de Pós-Graduação em Geoquímica e Geotectônica.

Área de concentração: Geoquímica dos Processos Exógenos

Orientador: Prof. Dr. Francisco William da Cruz Junior

São Paulo
2021

Serviço de Biblioteca e Documentação do IGc/USP

Ficha catalográfica gerada automaticamente com dados fornecidos pelo(a) autor(a)
via programa desenvolvido pela Seção Técnica de Informática do ICMC/USP

Bibliotecários responsáveis pela estrutura de catalogação da publicação:
Sonia Regina Yole Guerra - CRB-8/4208 | Anderson de Santana - CRB-8/6658

Della Libera de Godoy, Marcela Eduarda
Climate and environmental changes in southwestern Amazon Basin over the last 3000 years based on speleothem isotope records / Marcela Eduarda Della Libera de Godoy; orientador Francisco William Cruz Junior. -- São Paulo, 2021.
67 p.

Dissertação (Mestrado - Programa de Pós-Graduação em Geoquímica e Geotectônica) -- Instituto de Geociências, Universidade de São Paulo, 2021.

1. Paleoclima. 2. Amazônia. 3. Espeleotemas. 4. isótopos estáveis. 5. Sistema de Monção Sul-Americano. I. Cruz Junior, Francisco William , orient. II. Título.

UNIVERSIDADE DE SÃO PAULO
INSTITUTO DE GEOCIÊNCIAS

Climate and environmental changes in southwestern Amazon Basin over the last 3000 years based on speleothem isotope records

MARCELA EDUARDA DELLA LIBERA GODOY

Orientador: Prof. Dr. Francisco William da Cruz Junior

Dissertação de Mestrado

Nº 878

COMISSÃO JULGADORA

Dr. Francisco William da Cruz Junior

Dr. James Emiliano Apaéstegui Campos

Dra. Marília Harumi Shimizu

SÃO PAULO
2021

AGRADECIMENTOS

Agradeço primeiramente aos meus pais, Rita e Manoel, ao meu irmão, Danilo, e à minha irmã que ganhei da vida, Maria Alice, por todo amor, suporte, incentivo, torcida, compreensão e apoio que me deram durante a vida, em todos os momentos, incondicionalmente.

Agradeço ao meu compnaheiro, Julio Cauhy Rodrigues, por toda parceria, companhia, apoio, paciência e dedicação, tanto durante todas as etapas deste trabalho quanto na vida. Obrigada por todas as risadas, sonhos, viagens, aventuras, cavernadas, tatames, perrengues, experiências, chocolates e cafés compartilhados sempre.

Agradeço ao meu orientador Prof. Dr. Francisco William da Cruz por todo ensinamento, orientação, discussões e por todas as oportunidades e possibilidades que me apresentou na paleoclimatologia.

Agradeço ao Dr. Valdir F. Novello por toda ajuda, todas as reuniões, conversas, parceria, dedicação, orientação, conselhos, suporte e conhecimento para a realização deste trabalho.

Agradeço às (aos) minhas (meus) companheiras(os) e colegas de laboratório Melissa, Verônica, Angela, Plácido, Vanessa, Nathália, pelo companheirismo, apoio e suporte. Em especial, agradeço à Giselle Utida, além de tudo, pela amizade, pelos risos, por todo suporte e parceria, e ao Pânico (Nicolás Strikis), pelas viagens, conversas, discussões e conhecimento transmitido.

Agradeço o apoio dos envolvidos no Laboratório de Isótopos Estáveis (LES-CPGEO) do IGc/USP, ao Lawrence Edwards pela oportunidade de trabalhar nos laboratórios da Universidade de Minnesota (EUA) onde foram feitas as análises geocronológicas, ao Dr. José Leandro Campos pela ajuda com a parte estatística do trabalho, à Rebecca Orrison pela realização dos modelos climáticos e pela amizade que surgiu dessa parceria, ao Prof. Dr. Mathias Vuille pela colaboração imprescindível nesse trabalho, pela revisão do artigo e pelas discussões, e ao Evandro Girotto que realiza as coletas de água de chuva ao lado da caverna.

Este trabalho foi possível de ser realizado graças à Fundação de Amparo à Pesquisa do Estado de São Paulo (FAPESP), a qual fomentou a pesquisa em questão com a bolsa de mestrado vinculada ao processo número 2018/25020-8, e com o estágio de pesquisa no exterior (BEPE; 2019/22711-2) assim tornando possível e viável a realização desta pesquisa.

Sou extremamente grata a todas as pessoas que, direta ou indiretamente, fizeram parte da minha formação e deste trabalho.

AKNOWLEDGMENTS

First, I thank my parents, Rita and Manoel, my brother, Danilo, and my sister that I gained from life, Maria Alice, for all the love, support, encouragement, cheering, understanding and support they have given me during my life, at all times, unconditionally.

I thank my life partner, Julio Cauhy, for all the partnership, company, support, patience, and dedication, both during all the stages of this work and in life. Thanks for all the laughs, dreams, trips, adventures, caves, mats, chocolates, and coffees always shared.

I thank my supervisor Prof. Dr. Francisco William da Cruz for all the teachings, guidance, discussions, and for all the opportunities and possibilities that he presented to me in paleoclimatology.

I thank Dr. Valdir F. Novello for all the help, all the meetings, conversations, partnership, dedication, guidance, advice, support and knowledge to accomplish this work.

I thank my friends and lab mates Alyne, Melissa, Verônica, Angela, Plácido, Vanessa, Nathália, for the companionship and support. In special I thank Giselle Utida, beyond everything, for her friendship, for the laughs, for all the support and partnership, and Pânico (Nicolás Strikis), for the trips, conversations, discussions, and knowledge transmitted.

I thank the support of those involved in the Stable Isotopes Laboratory (LES-CPGEO) at IGC/USP, to Lawrence Edwards for the opportunity to work at the laboratories of the University of Minnesota (USA) where the geochronological analyses were done, to Dr. José Leandro Campos for his help with the statistics, to Rebecca Orrison for conducting the climate models and for the friendship that arose from this partnership, to Prof. Dr. Mathias Vuille for his indispensable collaboration in this work, for reviewing the article and for the discussions, and to Evandro Girotto for collecting rainwater next to the cave.

This work was only possible due to the Fundação de Amparo à Pesquisa do Estado de São Paulo (FAPESP), which fomented this research project with a master's fellowship (process number 2018/25020-8) and with the internship abroad program (BEPE; 2019/22711-2) making this work possible and feasible.

I am extremely grateful to all the people that, directly or indirectly, were part of my formation and of this work.

“Tomar o mundo nas mãos e agir com ele
de um modo inspirado e fortalecedor da alma
é um poderoso ato do espírito selvagem.”

Clarissa Pinkola Estés

RESUMO

DELLA LIBERA, M.E.G., 2021, Mudanças climáticas e ambientais no sudoeste da Bacia Amazônica nos últimos 3000 anos documentadas por registros isotópicos em espeleotemas, Brasil [Dissertação de Mestrado], São Paulo, Instituto de Geociências, Universidade de São Paulo, 67 p.

A variabilidade do Sistema de Monção Sul-Americano (SMSA) é de extrema relevância para a compreensão dos padrões climáticos na América do Sul, uma vez que é o principal regime de precipitação na maior parte do continente. O SMSA ocorre durante o verão e primavera austral associado a um grande influxo de umidade do oceano Atlântico tropical para o continente e a formação de uma zona de convecção no sudoeste da bacia amazônica, no eixo central da região das monções. Mudanças passadas no SMSA vem sendo documentadas através da análise de isótopos de oxigênio (δ^{18}O) em espeleotemas, que se tornou um dos principais indicadores geológicos (*proxies*) de mudanças paleoclimáticas continentais. O presente estudo faz uma reconstituição das mudanças climáticas e ambientais do sudoeste da Bacia Amazônica ocorridas nos últimos 3000 anos, com base nos registros isotópicos de δ^{18}O e δ^{13}C de alta resolução temporal, em espeleotemas da Gruta da Cuíca (Pimenta Bueno-RO), precisamente datados pelo método U/Th. A partir de dados obtidos em um programa de monitoramento isotópico e ambiental executado na área da caverna foi demonstrado que o sinal isotópico da água de infiltração não é significativamente afetado durante a percolação pelo epikarst, evidenciando que o registro δ^{18}O pode ser usado para rastrear informações paleoclimáticas e, portanto, variações do SMSA. As razões isotópicas do oxigênio do $CaCO_3$ dos espeleotemas estão relacionadas ao ciclo meteórico da água, sendo associadas principalmente a variação na quantidade de chuva e ao fracionamento que ocorre ao longo da trajetória de transporte da umidade. O registro de δ^{18}O da Cuíca revela três períodos climáticos da SMSA caracterizados por condições mais estáveis no primeiro milênio do registro de 3000-2000 A.P. (antes do presente), uma fase seca na Anomalia Climática Medieval (ACM) entre 1250-700 A.P., e nova fase úmida entre 500-150 A.P. durante a Pequena Idade do Gelo (PIG). A comparação dos dados da Cuíca com estudos anteriores na América do Sul revelou evidências de um dipolo de precipitação Leste-Oeste na Bacia Amazônica, principalmente durante a intensificação da atividade do SMSA, como na PIG. Os dados de δ^{13}C e δ^{18}O são fortemente correlacionados e indicam que o os processos de produção biogênica no solo podem ser atrelados as variações de precipitação. Os dados isotópicos dos espeleotemas estudados foram também utilizados na investigação da relação entre a dinâmica populacional das culturas pré-colombianas do sudoeste da Amazônia com as mudanças paleoclimáticas e ambientais ocorridas na região. Análises estatística de séries temporais dos dados de δ^{18}O indicam uma persistente variabilidade multidecenal na intensidade do SAMS, as quais estão possivelmente associadas com a influência dos modos de variabilidade decenais e multidecenais do Atlântico. Os novos registros de alta resolução δ^{18}O e δ^{13}C apresentados aqui contribuem, portanto, para avaliar melhor as variações e intensidades do SMSA de forma contribuir para o melhor entendimento de como a dinâmica climática na porção central da SAMS na Amazônia estão associadas afeta as condições hidrológicas na periferia do domínio.

Palavras-chave: espeleotemas, isótopos estáveis, paleoclima, paleoambiente, Sistema de Monção Sul-Americano, Amazônia.

ABSTRACT

DELLA LIBERA, M.E.G., 2021, Climate and environmental changes in southwestern Amazon Basin over the last 3000 years based on speleothem isotope records, Brazil [Master's Thesis], São Paulo, Instituto de Geociências, Universidade de São Paulo, 67 p.

The variability of the South American Monsoon System (SAMS) is of uttermost relevance for understanding climate patterns over South America since it is the most important precipitation regime acting over the continent. The SAMS occurs during austral summer and spring due to a major influx of vapor from tropical Atlantic Ocean into the continent, when a zone of deep convection is then established over southwestern Amazon basin, at the monsoon core region. Past monsoon changes have been documented through oxygen isotope analysis ($\delta^{18}O$) from speleothems and became one of the main proxies utilized to retrieve continental paleoclimatic data. The results from monitoring program performed at the cave site indicate that the incorporation of oxygen isotopes in the $CaCO_3$ of speleothem's formation is closely linked to the meteoric water cycle in the region, holding relevant information about local rainfall amount and precipitation along the moisture transport from ocean to continent. However, the patterns of SAMS for last millenniums have not yet been deeply discussed for the Amazon region. The current work is based on high resolution speleothem isotope records from Cuíca cave (Pimenta Bueno-RO) that were used to reconstruct paleoclimatic and paleoenvironmental records from Southwestern Amazon Basin for the last 3000 years. Cuíca speleothem $\delta^{18}O$ record reveals three climatic periods in the SAMS characterized by wetter, drier and wetter climate corresponding to the e first millennia of the record from 3000-2000 B.P., the Medieval Climate Anomaly (1250-700 B.P. - MCA) and Little Ice Age (500-150 B.P. - LIA), respectively. In addition, comparison of Cuíca cave data with previous studies from South America brought up new evidence of an east-west precipitation dipole over the Amazon Basin, mainly during intensifications in SAMS activity, as identified in the LIA climate event. A high correlation between $\delta^{13}C$ and $\delta^{18}O$ data is here interpreted as a response of biogenic CO_2 production in soil to changes in precipitation. Both $\delta^{13}C$ and $\delta^{18}O$ records are used here to check if the population dynamics of pre-Columbian cultures from Southwestern Amazonia are related with paleoclimatic and paleoenvironmental changes in the region. Statistical analysis of $\delta^{18}O$ record reveal persistent decadal and multidecadal variability in SAMS intensity associated with Atlantic ocean climate modes. In summary, the new high-resolution $\delta^{18}O$ and $\delta^{13}C$ records from southwestern Amazon contributes to further assess monsoon variations at its core region to better understand the impact of atmospheric circulation in Amazon on hydrological conditions over the periphery of SAMS domain.

Keywords: speleothems, stable isotopes, paleoclimate, paleoenvironment, South American Monsoon System, Amazon.

SUMMARY

LIST OF FIGURES

1. PREAMBLE

1.1. Dissertation Format

The current master's degree dissertation is presented in seven sections. The first topic comprises the dissertation format and the research aims. The second is an introduction about the speleothem formations in caves and the climatic meaning of its isotopic signatures, a brief description of the study area and Cuíca cave (Pimenta Bueno-RO), and modes of climate variability. The third section presents the methods employed in this research, and the fourth section comprises results and discussions in the format of the full-length article named: "Amazonian lowlands paleoclimatic variations over the last three millennia and its implications for pre-Columbian populations" to be submitted to an international periodic. The fifth and sixth sections contain the results and a brief discussion of the statistical analysis and modes of variability that were not discussed in the article, respectively. The following topic presents this work's final considerations, which gathers the conclusions of both the paper and the additional statistical analysis discussions.

1.2. Research Aims

The current research goals are listed below:

- To reconstruct hydroclimatic and vegetation changes over the last three millennia in the study area from analysis of $\delta^{18}O$ and $\delta^{13}C$ of speleothems from Cuíca cave.
- To identify climatic patterns of the SAMS and SACZ during the last three millennia.
- To investigate possible mechanisms for climatic changes over Amazon basin during the considered period by comparing the novel $\delta^{18}O$ record from Cuíca cave with previously published $\delta^{18}O$ records in adjacent regions in Amazon basin and South America.
- To identify paleo-pluviosity patterns and trends in different time scales, from interannual to centennial, by applying statistical analysis for time series in the $\delta^{18}O$ record.
- To analyze the hydrochemistry conditions and signatures from collected rainwater in the monitoring station near the cave site and collected drip water in order to calibrate the speleothems isotopic records against the current climatic fluctuations.

2. INTRODUCTION

2.1. Formation of Speleothems

Speleothems are secondary mineral deposits formed in caves that can occur in various forms, such as stalagmites, stalactites or flowstones. Stalagmites have been used as a great paleoclimate archive, mostly because of its potential to record environmental and climate proxies, the precise U/Th dating method used for speleothems, and because of its simple stratigraphy resulting of the precipitation of successive calcite layers from cave drip water. Its formations is then associated to a sequence of chemical processes that occur from the rainwater interaction with the soil all the way to the interior of the cave (Lauzitzen & Lundberg, 1999). Initially, the water from the ocean is evaporated and advected into the continent, where it might lead to cloud formations and eventually condensate into rainfall. The rainwater then percolates through the soil, where the partial pressure of CO_2 (P_{CO_2}) is higher relative to the water (unsaturated in CO_2) due to organic matter decomposition, leading to the dissolution of CO_2 and yielding in the formation of carbonic acid (H_2CO_3). The carbonic acid is a weak acid, which will then gradually dissociate into other carbon chemical compounds at higher pH to bicarbonate (HCO_3^-) and carbonate (CO_3^{2-}), also known as dissolved inorganic carbon (DIC), according to the following chemical reactions (Fairchild and Baker, 2012):

$$H_2O + CO_2 \leftrightarrow H_2CO_3 \qquad \text{- Reaction 1}$$

$$H_2CO_3 \leftrightarrow HCO_3{}^- + H^+ \qquad \text{- Reaction 2}$$

$$HCO_3{}^- \leftrightarrow CO_3{}^{2-} + H^+ \qquad \text{- Reaction 3}$$

The solution pH value will determine the proportions of DIC species, but at near-neutral pH values, the HCO_3^- is the dominant DIC (Fairchild & Baker, 2012). This solution then gradually becomes more acidic due to its interaction with CO_2 as it percolates through the soil, until it reaches the fissured and weathered limestone above the vadose zone, the epikarst, and eventually the limestone bedrock. The resulting acid solution dissolves the carbonate rock according to the following reaction:

$$CaCO_3 + H_3O^+ \leftrightarrow Ca^{2+} + HCO_3^- + H_2O \qquad \text{- Reaction 4}$$

The equilibrium reaction of the entire dissolution of the carbonate can be described as:

$$H_2O + CO_2 + CaCO_3 \leftrightarrow Ca^{2+} + 2HCO_3{}^{-} \qquad \text{- Reaction 5}$$

Therefore, as the solution percolates through the limestone bedrock, it becomes saturated in Ca^{2+} as Reaction 5 is constantly happening, until it reaches the cave atmosphere, which is usually much lower (P_{CO_2}) than the solution depending on the ventilation of the cave. This leads to the progressive degassing of CO_2 from the solution to the cave atmosphere through molecular diffusion (Dreybrodt, 2008) and the water subsequently becomes supersaturated in calcium carbonate, resulting in the $CaCO_3$ precipitation forming the speleothems.

The CO_2 degassing can occur during some stages of the water path: still within the bedrock before it reached the cave environment but already in contact with the cave atmosphere; due to a longer residence time of the water drop on the cave ceiling or stalactite, thus leading to the precipitation of these speleothems; when the water drop hits the stalagmite apex it loses CO_2 molecules to the atmosphere due to the impact and the subsequent thin layer of water on the cave floor or already the stalagmite will degas, successively precipitating $CaCO_3$ layers (Dreybrodt, 2008).

2.2. Oxygen and Carbon Stable Isotope Records

The most common proxy record employed for paleoclimatic studies based on stalagmites is the oxygen isotope records ($\delta^{18}O$), first due to its relative straight link with climate since the oxygen incorporated in the speleothem's formation comes from the rainwater and it might bring a more straightforward interpretation to this proxy in comparison with others; and second, to the fact that it is stable over time, thus retaining important information about the rainwater (Lachniet, 2009).

The phase changes of water in the different stages of the hydrologic cycle are accompanied by oxygen isotope fractionation, a process where one isotope is favored over the other in the flux between reservoirs, thus favoring one isotope over the other according to their mass, as the following equation (Clark & Fritz, 1997):

$$\alpha = {}^{Ra}/_{Rb} \qquad \textbf{Eq. 1}$$

E. g.

$$\alpha^{18}O_{(water-vapor)} = {}^{(^{18}O/\,^{16}O)_{water}}\!\Big/_{(^{18}O/\,^{16}O)_{vapor}}$$

where α is the fractionation factor and R is the isotopic ratio of less/more abundant of the element.

However, to evaluate the relative variations between the isotope ratios, the notation δ is used as pointed out in Eq. 2, showing the relation between the isotope ratio of the sample and the isotope ratio of an international reference standard, establishing the isotopic ratio of the sample relative to that of the a standard according to the equation (Lachniet, 2009):

$$\delta^{18}O_{sample} = \frac{\left(\frac{^{18}O}{^{16}O}\right)Sample - \left(\frac{^{18}O}{^{16}O}\right)Standard}{\left(\frac{^{18}O}{^{16}O}\right)Starndard} \times 1000 \qquad \textbf{Eq. 2}$$

The δ values are expressed as the difference in parts per thousand or permil (‰) from the reference value to facilitate the use of outcomes from this equation, which are rather small. For calcium carbonate, the standard value used as reference is the Vienna Peed Dee Belemnite (VPDB), and in the case of water, the VSMOW (Vienna Standard Mean Ocean Water) is the internationally adopted standard. Both standards are established as 0‰ in a way that the variations in the $^{18}O/^{16}O$ ratio obtained in carbonate or water samples are always relative to differences from the standard, meaning that the $\delta^{18}O$ values from a sample are “enriched” with ^{18}O when the values are positive (higher $^{18}O/^{16}O$ sample ratio relative to the standard), or “depleted” of ^{18}O (lower $^{18}O/^{16}O$ sample ratio relative to the standard) (Lachniet, 2009).

From a statistical perspective of reactions in thermodynamic equilibrium and in constant rearrangement of bonds, as is the case here, stronger chemical bonds are more likely to be harder to break relative to weaker ones (Clark & Fritz, 1997). In condensation processes, for example, the lighter (heavier) water isotopologues, i.e., H_2O^{16} (H_2O^{18}), will tend to remain in the vapor (liquid) phase, such as the condensation of water vapor into rainwater, in which a greater amount of heavier isotopologues tend to be incorporated. Therefore, the ^{18}O isotope is favored over the ^{16}O in condensation processes, thus rainwater will have higher $\delta^{18}O$ relative to the remaining cloud vapor. The opposite behavior is observed in evaporation processes, such as the evaporation of the ocean surface (liquid) into the atmosphere (vapor), when then the heavier water isotopologues (H_2O^{18}) tend to remain in the liquid phase (ocean) and larger quantities of the lighter isotopologues (H_2O^{16}) are incorporated into the vapor phase (Lachniet, 2009; Clark & Fritz, 1997). This flux between reservoirs then fractionates the water $\delta^{18}O$, which is mostly related to the temperature in which the phase changes occur and the consequent energy required to break the bonds that can be established by:

$$1000 ln\alpha_{(water-vapo\ )} = 1.137(10^6/T_k{}^2) - 0.4156(10^3/T_k) - 2.0667 \textbf{ Eq. 3}$$

where T is for temperature of the phase change in Kelvin. This means the temperature needs to decrease for condensation processes to occur, and increase for evaporation to occur. Therefore, the climatic signal obtained from speleothems in cave systems can be retrieved due to these processes that occur on the water pathway between the ocean, to meteoric water and finally the precipitation of speleothems in caves (Fig. 2.2-1). The water is evaporated from the ocean surface and the vapor is the advected over the continent, where it eventually condenses and falls as rainwater. The water then percolates the soil, epikarst and finally enters the cave environment as drip water from which calcite is deposited (Lauritzen and Lundberg, 1999). A summary diagram is presented below:

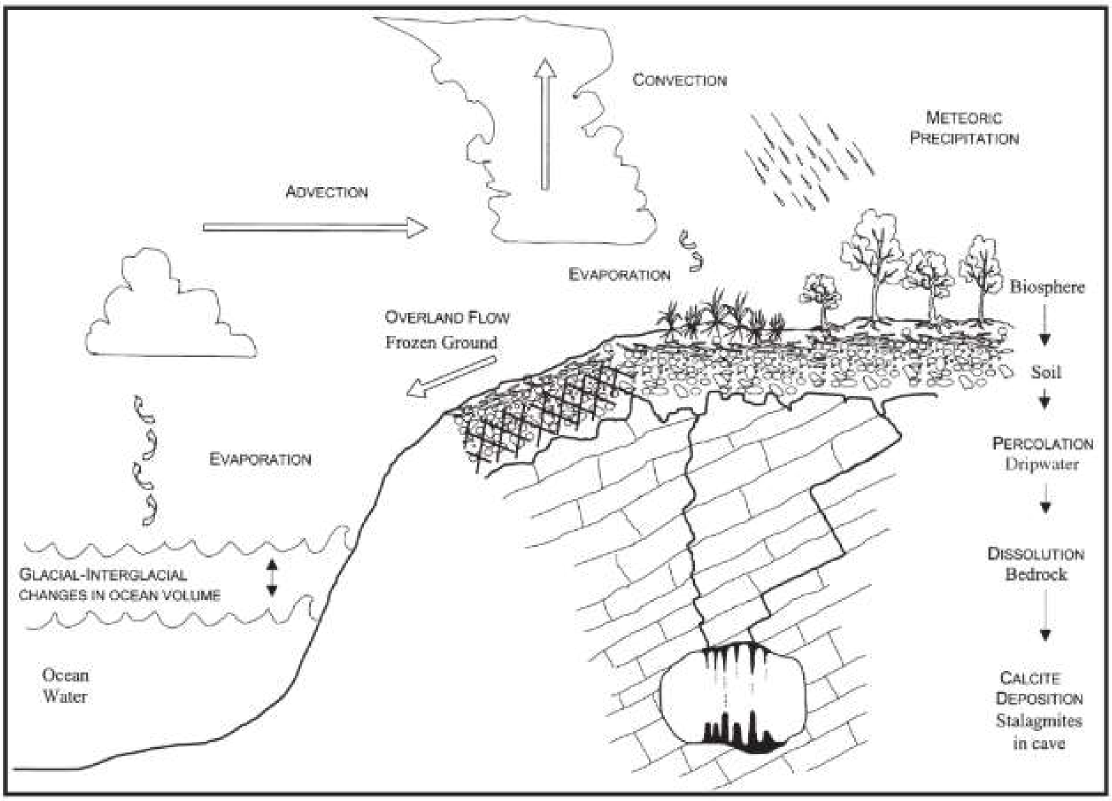

Figure 2.2-1 - Speleothem and the meteoric cycle. Glacial to interglacial changes in sea level, and thus chemistry, are indicated to the left. Advection carries water vapour varying distances, and convection will alter its elevation and thus the site of rain formation. Rainwater travels through the biosphere and is modified therein; it may percolate into, or be evaporated from, the surface or it may be forced into overland flow by a frozen substrate. Percolation waters pick up CO_2 and $CaCO_3$ en route, by various possible paths, to the cave. Stalactites and stalagmites are deposited in the low P_{CO_2} of the cave gallery. The resulting cave calcites contain various environmental signatures, like isotope composition

($\delta^{18}O$, $\delta^{13}C$, and $\delta^{2}H$), recurrent laminae or bands, trace element composition, and crystallographic changes. *Image from : Lauritzen and Lundberg (1999).*

As for the $\delta^{13}C$, the values of drip water and the precipitated calcite layer over a stalagmite are affected by other processes that lead to the fractionation of the carbon stable isotopes, both external (e.g. type of vegetation above the cave and soil P_{CO_2}) and internal (e.g. residence time of the water in the soil and rock) factors (Scholz, Mühlinghaus, & Mangini, 2009). Initially, the source of carbon that will ultimately precipitate as speleothems is the CO_2 from both plant root respiration and decomposition of organic matter by biological activity in the soil (leading o high P_{CO_2} in the soil), which is then dissolved into the rainfall infiltration water (unsaturated in CO_2) that continues to percolate through the cave host-rock and eventually reaches the cave (Dreybrodt, 2008; Novello et al., 2021). The acid solution acts dissolving the cave host-rock (Reactions 1-4), an interaction that usually occurs in an intermediate condition between an open and closed system, meaning the solution is in a state where it is in a partial equilibrium with CO_2 reservoir from the soil (open system) and the CO_2 present in the solution is continuously being consumed as it dissolves the host-rock until it is in Ca^{2+} equilibrium (close system) (Fairchild & Baker, 2012; Fohlmeister et al, 2020; Novello et al., 2021).

Both plant root respiration and decomposition of organic matter by biological activity in the soil can significantly contribute to the isotopic composition of the speleothem's formation. This way, $\delta^{13}C$ can reflect changes in the biological activity, the amount of biomass and type of vegetation above the cave by producing more negative values. The type of dominant plants above the cave can thus print an isotopic signal to the speleothems $\delta^{13}C$ due to a kinetic fractionation process during photosynthesis, where plants typically from savanna and grasslands (C4 photosynthetic pathway) present a $\delta^{13}C$ range between -15 to -10‰, plants typical of dense forests (C4 photosynthetic pathway) showing a $\delta^{13}C$ typically ranging from -30 to -24‰, or CAM plants that present $\delta^{13}C$ values that overlap the carbon isotopic signature of both C_4 and C_3 plants (Hendy, 1971; Silva et al, 2008; Fohlmeister et al, 2020; Pessenda et al, 2010, Novello et al., 2021; Dreybrodt, 2008).

Furthermore, the interaction with the rock is one of the processes that affects the carbon isotope signature of the drip water, what may vary according to the dissolution path of the solution (Dreybrodt, 2008; Novello et al., 2021). A process that can affect $\delta^{13}C$ values is the precipitation of calcite prior to the drip water reaching the stalagmite apex, such as in the fractures of the host-rock or already in the cave environment when stalactites are formed. This process is named as prior calcite precipitation (PCP) and the degree in which PCP occurs can vary due to the difference in P_{CO_2} from the solution and the air it is in contact with, either in the fractures or already in the cave environment, and the residence time of this water in the host-rock fractures and consequently the time this solution is in exposed to the air in the epikarst or the cave atmosphere as drip water before it actually drips (Fairchild & Baker, 2012; Fohlmeister et al, 2020). The time of residence of the solution in the epikarst can be influenced by hydrological availability, where wetter (drier) conditions decrease (increase) the time of residence due to a higher (lower) recharge in the aquifer and that influences the time in which the solution is in contact with the air in the epikarst and also influences in the absence (presence) of air in the epikarst, decreasing (increasing) the degassing and consequently increasing (decreasing) PCP rates. High PCP rates (longer residence time and longer contact with the cave atmosphere) tend to remove the heavier CO_2 isotopologues (^{13}C), what is thus reflected in the stable isotope record from the stalagmite as an increase in $\delta^{13}C$ values.

Furthermore, the cave atmosphere can also impact the $\delta^{13}C$ of speleothems due to variations in atmospheric parameters such as P_{CO_2}, humidity, ventilation, and drip rate. These atmospheric parameters can modulate the rate of degassing and evaporations, and in case of rapid loss of CO_2 the isotopic signal from kinetic fractionation between HCO_3^- and CO_2 (aq) can be printed in the speleothem $\delta^{13}C$ values, and in this conditions the speleothem cannot be used to give paleoclimate data (Hendy, 1971).

Despite of the complexity of a climatic or environmental interpretation due to the presence of several processes involved in the modulation of speleothems $\delta^{13}C$ values, some studies have pointed a dominant control on $\delta^{13}C$ of speleothem associated with processes in soil such as of CO_2 released by plant roots and microorganism respiration (Cruz et al., 2006; Novello et al., 2019, 2020; Utida et al., 2020). Multiproxy approach can also contribute to the interpretation of the $\delta^{13}C$ in speleothems, such as presented by Utida et al (2020), where the comparison between several hydrological and vegetation proxies allowed the authors to associate variations in $\delta^{13}C$ from the speleothems to changes in vegetation.

2.3. Monitoring Program

One of the greatest challenges in the interpretation of paleoclimate records based on speleothems is the understanding of how environmental changes occurring on each individual cave system is related with changes on the *proxies* recorded within the speleothems, such as stable isotopes, trace elements, organic matter, among others. Therefore, to have a monitoring study is vital to understand the effects of environmental and climatic changes on speleothem's proxies and then to better interpret the paleoclimatic information (Fairchild et al., 2006). Hence, several studies have been approaching this subject in different perspectives such as drip water hydrochemistry (Cruz et al., 2005b; Karmann et al., 2007), comparing the $\delta^{18}O$ values of modern speleothem calcite with $\delta^{18}O$ values predicted by a proxy system model (Carlson et al., 2020), developing a method of resolving rainfall-recharge thresholds in karst (Baker et al., 2020), and so on. For the current research, stable isotope analysis were made for rainwater and drip water ($\delta^{18}O$ and δD), and for modern calcite precipitated in watch glasses ($\delta^{18}O$ and $\delta^{13}C$).

2.4. Study Area

This research was based on stalagmites from Cuíca cave (-11°40'S, -60°38'W, ~310 m a.s.l.) on southwestern Amazon basin, located in Pimenta Bueno city (RO), Brazil. Cuíca cave is embedded in the limestones of Pimenta Bueno Formation from the Paleozoic era, Ordovician-Silurian period (ca. 495-417 Ma – Oliveira, 2015) (Fig. 2.4-1), and is one of the few limestone caves in southwestern Amazon basin given the limited occurrence of carbonate formations in the region (Rizzotto & Quadro, 2007; Oliveira, 2015). Cuíca cave has a development of ~200 m with a mostly rectilinear pattern without major unevenness, a small river runs within the cave system, and a 1 m high river conduct leads to the gallery where the speleothems were collected (Fig. 2.4-2). The gallery has ~15m in length and is characterized by a major collapsed ceiling pile, thus yielding in an ~4m unevenness between the river and the level of the speleothems formations. It is well-ornamented with speleothems, whereof several have active dripping and are currently forming. The relative humidity in the cave is always at 100% level and temperature around 25°C. The site is directly affected by the SAMS, characterized by heavy rainfall from October-April, what might eventually increase the river level to the point of filling the river conduit and reaching the collapsed ceiling hall during extreme events.

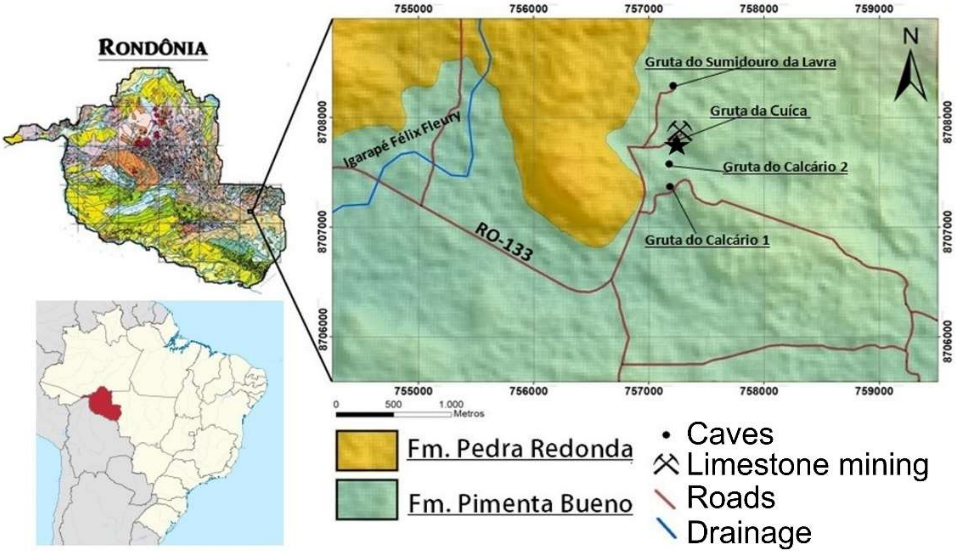

Figure 2.4-1 – Study area map showing the cave location (black star).

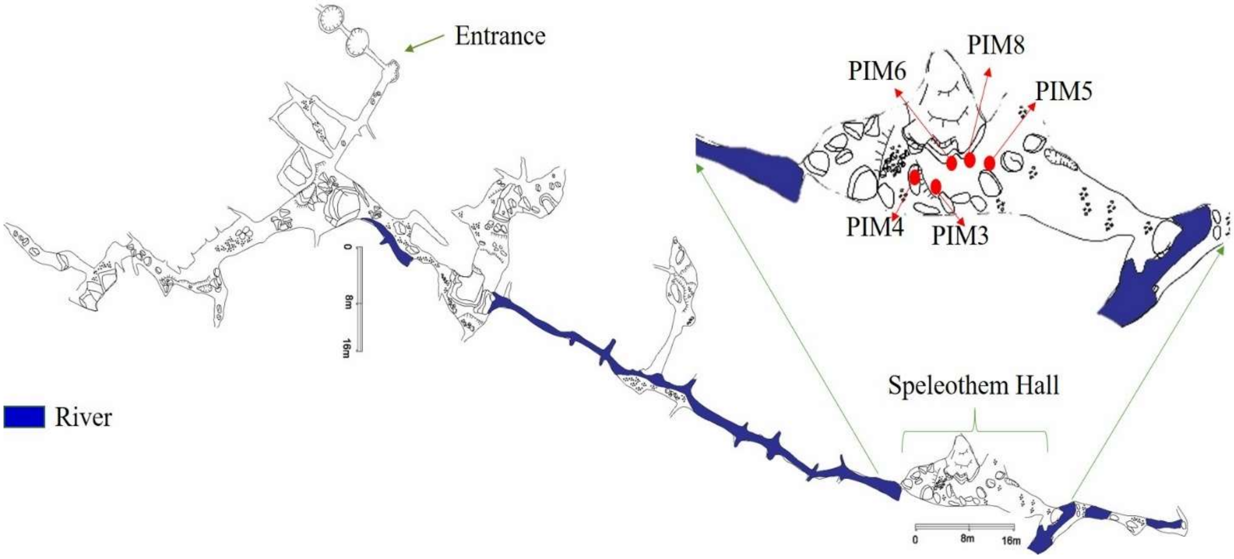

Figure 2.4-2 – Cuíca cave map (made by Spelayon Consultoria) with indication of the sites form where the stalagmites used in this study were collected.

2.5 Modes and Patterns of Climate Variability in the Atlantic and Pacific oceans

The Atlantic and Pacific oceans are important climatic modulators for the South American climate, and both oceans go through periodic fluctuations in sea surface temperature (SST). In the Atlantic ocean, a multidecadal oscillation with a timescale between 60-80 years has been given the name of Atlantic Multidecadal Oscillation (AMO) (Alexander et al, 2014; Knight et al, 2006; Kerr, 2000; Knudsen et al., 2011). This oscillation is based on temperature variations over large regions of North Atlantic that shift between cold and warm phases, determined as negative and positive phases, respectively (Alexander et al, 2014). As this oscillation is linked with SSTs from North Atlantic, several processes might play a role in these variations, such as changes in heat flux between north and south Atlantic oceans, amount of ice in north Atlantic, wind currents that affect ocean currents, and the changes in strength of the Atlantic Meridional Overturning Circulation (AMOC) (Alexander et al., 2008; Knight et al., 2006; Knudsen et al., 2014).

Several studies have investigated recent (last ~150 years) AMO cycles based on instrumental data to better understand this oscillation (Knudsen et al., 2011), however longer time records of this variability are necessary to reconstruct it over time and thus accurately characterize it. In order to do that, a number of multiproxy datasets (speleothems, tree rings, ice cores, lake sediments, etc.) along with climate models and statistical methods are gathered and analyzed, yielding an AMO index (e.g. Mann et al., 2009; Gray et al., 2004). Moreover, these changes have been associated with climatic effects on continental regions, in particular South America, as documented by previous studies such as Bird et al. (2011) and Novello et al. (2012) that document changes in SAMS due to AMO shifts over the Andes and Northeastern Brazil (NEB), respectively.

In addition to the AMO, the North Atlantic Oscillation (NAO) is another phenomenon that occurs over Northern Hemisphere that has significant effects over climatic patterns in the Atlantic region. The NAO is characterized by a see-saw atmospheric mass over Arctic and the subtropical Atlantic, modifying Atlantic wind speed, direction, and altering heat and moisture distribution provided by the Atlantic ocean to the continents (Hurrell et al., 2003; Trouet et al., 2009). When NAO is in a positive phase, a strong poleward low-level jetsteam occurs over North Atlantic, mainly during Northern Hemisphere winter (DJF) due to an enhanced low pressure zone over the Artic combined with a high pressure zone over subtropical Atlantic, moving this atmospheric mass (Hurrell et al., 2003; Martineau et al., 2020). On the other hand, both atmospheric zones are weakened during NAO negative phase.

However, contrary to AMO, the NAO implications for South American climate have not been yet extensively discussed in previous studies, as most studies about NAO are addressed to Northern Hemisphere. Some studies regarding NAO effects over South America focus on precipitation changes over NEB (Kayano & Andreoli, 2004; Rao & Brito, 1985), which relate positive (negative) NAO phases with wetter (drier) conditions over NAO, and Souza & Cavalcanti (2009) expatiate on how NAO variations between phases and/or intensity affect temperature changes in tropical south Atlantic and, in turn, NEB precipitation. Trouet et al. (2009) gives a general idea on the several atmosphere-ocean interactions and circulations that could lead to climatic changes such as the Medieval Climate Anomaly (MCA), and associates the persistent positive NAO phase during MCA with a drought on western South America.

For the Pacific ocean, one of the most discussed climatic phenomenon for South America is the El-Niño Southern Oscillation (ENSO). It is the main mode of natural climate variability on interannual time scales (2-7 years) characterized by changes in the sea surface temperature (SST) in the tropical Pacific, where warmer (positive phase) or colder (negative phase) than average temperatures define El Niño or La Niña events, respectively (Lu et al., 2018; Cai et al., 2020). Those events are associated with ocean-atmospheric interactions. An initial warming in eastern equatorial Pacific SSTs leads to a weakening of the oceanic equatorial upwelling due to the reduced surface pressure and trade wind strength, thus amplifying the initial warming, and eventually resulting in an El Niño event (warmer than average SST in tropical Pacific). For the La-Niña events, the opposite condition is observed, thus colder than average SSTs in tropical Pacific are detected (Lu et al., 2018; Cai et al., 2020).

The episodic warming and cooling of SSTs can generate unusual weather patterns, such as precipitation or temperatures anomalies around the world through atmospheric teleconnections (Lu et al., 2018). For South America, during positive ENSO phases (El Niño) wetter conditions prevail over westernmost and south-eastern regions in South America, while negative rainfall anomalies are observed over eastern Amazon Basin and north-east Brazil (NEB). On the other hand, negative ENSO phases (La Niña) lead to positive rainfall anomalies over northern South America (Cai et al.; 2020). Yet, for southwestern Amazon basin, our region of study, studies show interannual variability associated with ENSO, however they do not present statistically significant correlations between rainfall anomalies over the site and ENSO modes (Garreaud et al., 2009; Grimm & Tedeschi, 2009; Grimm & Saboia, 2015; Cai et al., 2020). Only in Grimm and Tedeschi (2009) the authors evidence that southwestern Amazon climate extreme signals during late autumn are usually opposite to that over eastern Amazon. Yet, spatial coherence over this region is lower since it lays in an intermediate zone and can thus be affected by the same mechanisms of areas to the north (northern Amazon/South America) or south (SESA/ low-level jet), or even experience the same dominant effects in both El Niño and La Niña events (Grimm & Tedeschi, 2009), what can be further observed in climate models from other studies (e.g. Garreaud et al., 2009; Grimm & Saboia, 2015; Cai et al., 2020).

Finally, decadal to multidecadal variabilities in the Pacific have been evidenced to affect ENSO, and therefore South American climate, such as the Pacifica Decadal Oscillation (PDO) and the Interdecadal Pacific Oscillation (IPO). The PDO is an important mode of multidecadal SST's variability in the extratropical North Pacific that have been characterized by cycles of both 50-70 years and of ~20-30 years (Biondi et al., 2001; MacDonald & Case, 2005; Kayano &Andreoli, 2007; Buckley et al., 2019). Its positive (negative) phase is characterized by warm (cold) SST's in northeastern Pacific along with a cool (warm) SST anomaly in the equatorial Pacific ocean, and its strength in both phases present fluctuations between 2-7 years, indicating an ENSO influence in this mode (Biondi et al., 2001; MacDonald and Case, 2005; Silva et al., 2011; Gamelin et al., 2020). The IPO, on the other hand, is characterized by a SST anomaly (SSTA) throughout the entire Pacific, featuring abrupt changes in SSTA patterns across the Pacific due to its phase reversals every 20-30 years within its cycle of 40-60 years. The IPO negative (positive) phase presents a La Niña-like (El Niño-like) cold (warm) SSTA over tropical Pacific (Dong & Dai, 2015; Buckley et al. 2019), and it also has a role in modulating global-mean temperature on (multi)decadal time scales (Dai et al., 2015). The IPO is considered to be a broader expression of PDO, therefore these two systems are highly correlated with each other, and their phase changes are linked with increased or decreased frequency of warm or cold phases of ENSO (Dong & Dai, 2015; Buckley et al. 2019).

When looking at these modes impacts on South American climate, some studies point to enhanced/reduced effects of ENSO according to different PDO phases, such as that the teleconnections of ENSO are stronger (weaker) for South America rainfall when it is in the same (opposite) phase as PDO (Kayano &Andreoli, 2007; Silva et al., 2011; Gamelin, et al., 2020). As for the IPO, Buckley et al. (2019) documents that, during positive IPO phases, the Amazon basin experiences a drought, while anomalous wet conditions prevail further to the south, whereas opposite conditions are observed for negative IPO phases. However, according to the composite analysis of this study, also observed in Dong and Dai (2015), southwestern Amazon also lays in an intermediate zone (as observed for ENSO), yet precipitation here behaves more as southern regions from the Amazon basin region as it is referred in the study, therefore positive (negative) IPO phases lead to wetter (drier) conditions over the current study site.

3. METHODS

3.1. Speleothem Chronology

The speleothems chronologies were obtained using U-series disequilibrium dating (U/Th method) at the Institute of Global Environmental Change at Xi'na Jiaotong University in China and also at Geochronology Laboratory of the University of Minnesota in the United States. The carbonate powder of the speleothems was collected at the Laboratório de Sistemas Cársticos at the Instituto de Geociências of Universidade de São Paulo (IGc-USP) using a Dremel rotatory tool attached to a flexible cable shaft. Glass vials were used to store the carbonate samples of approximately 0.1g, taken from the top of the speleothem downward. Sampling for geochronology was carried out following individual layers of the speleothem, using drills with an average diameter of 0.1mm and avoiding layers with detrital content (mud layers) as it could be a source of ^{232}Th from the clay minerals.

The chemistry preparation for collection of uranium and thorium of speleothems were performed in a super clean laboratory and the chemistry procedures used are divided in three steps and consist in (1) weight, spiking and sample dissolution; (2) Fe precipitation, centrifuge, and dissolution; (3) ion exchange columns.

(1) (Weight, sample dissolution and spiking) – A high precision scale is used to weight the powder samples. If the speleothem has previous U/Th analyses, it is used the concentration of ^{238}U and ^{234}Th to calculate the amount needed for the analyses. If there is no information about the concentrations, 0.5g of sample is used. A Teflon beaker is used to weight the sample, and after weighting is added a small amount of water to cover the powder and avoid loss of mass and contamination in the weight room. Before spiking, the sample is dissolved using HNO_3 (3 to 6 drops). The amount of Spike (solution content ^{236}U – ^{233}U – ^{229}U) added is calculated using a reference table with the sample ^{238}U concentration (if known). To finish the first step, $HClO_4$ is added (drops between 4 to 15 depending on the content of organics in the sample) and the Teflon beaker is closed and put to reflux (step used to homogenize the solution) on a hot plate at 150 ºC for 30 minutes, and after the reflux the solution is submitted to a completely dry down with the beaker open at a temperature between 200 ºC to 203 ºC for 3 to 6 hours until a milky solid form at the bottom of the beaker.

(2) (Th and U co-precipitation with Fe) Second step starts with the dissolution of the milky solid with 2N HCl and with the solution is pour in a centrifuge tube with Fe solution (2 drops). Ammonia (NH_4OH) is added (4 to 10 drops) until a rust color precipitate form (precipitate of heavy elements) and the sample is centrifuged for seven minutes at 2600 rpm. After a round of centrifuge, the supernatant is discarded, and SC (super clean) water is added. Two more rounds of centrifuge are performed repeating the process of discard the supernatant and adding SC water. The precipitate is dissolved with 7N HNO_3 and the solution is poured again in the Teflon beaker for a completely dry down on a hot plate at 200 ºC until a submillimeter precipitate form at the bottom of the beaker. A sequence of dry downs is performed after dissolving the solution with 2 drops of $HClO_4$ (first dry down) than 1 drop of 14N HNO_3 (second and third dry down). After the third dry down it is added 7N HNO_3, and the solution is ready for the ion exchange columns.

(3) (Ion exchange columns) – To separate and collect the thorium and uranium, SPECTRA/GEL® ION EXCHANGE 1x8 resin are prepared. SC water is added until fill the column volume and waiting until the all the water goes through the column, repeating this step two times and adding 1 drop of 14N HNO_3 in the second time. To finish the resin preparation, 7N HNO_3 is added until 2/3 of the column volume waiting until all the solution goes through the column. For the elution of the reagents, the sample solution is poured in the column and waiting until the sample is absorbed by the column. The column is filled with 7N HNO_3 two times with 2/3 of the column volume in the first time and 1/3 in the second time. All the solution collected until this step is discarded and a clean beaker is set under the column to start the thorium collection. For thorium collection, 6N HCl is added filling 2/3 of the column for two times, closing the beaker after the collection. For the uranium collection the Teflon beaker used in the previous chemistry steps (1 and 2) is set under the column, and the column is filled with SC water two times. Finishing the collection, 1 drop of $HClO_4$ is added to the solutions and the beakers are put to completely dry down on the hot plate at 203 ºC until a submillimeter solid precipitated. Three rounds of completely dry down are done after dissolving the solid with $HClO_4$ (before first dry down), and 1 drop of 14N HNO_3 (second and third dry down). The chemistry process is completed after adding ICP-MS standard solution (SC water with 1% 14N HNO_3 and 60 drops of HF), and the solutions are ready to be analyzed on the ICP-MS mass spectrometer.

An MC-ICP-MS (Multi-collector Inductively Coupled Plasma Mass Spectrometry) Finnigan Elements and Finnigan Neptune Type were used to analyze the samples solutions following the procedures stablished by Cheng et al. (2013). The age calculations were made using the isotopic ratios measured and corrections factors to eliminated effects of contamination by detrital Th^{232}, based on Edwards et al. (1986) and Richards & Dorale (2003).

3.2. Oxygen and Carbon Stable Isotopes Analyses

The stable isotopes analyses were performed using a gas source mass spectrometer model Delta Plus Advantage (Thermo Finnigan) coupled to a Finnigan Gas-Bench II automatic sample preparation system at the Stable Isotope Laboratory of the Center of Geochronology Research (LES-CPGEO) in the Institute of Geoscience of the University of São Paulo (IGC-USP). The speleothem carbonate samples were collected at the Laboratory of Karstic System in the Geoscience Institute from the University of São Paulo.

The sampling was made using a micromill with a drill bit diameter of 0.15mm, with steps of 0.2 to 0.4 mm according with the wanted resolution (considering a known chronology for the speleothem). The sampling profile follows the speleothem growth axis to avoid samples subjected to kinetic fractionation process. A pair of Hollenbeck is used to collect approximately 0.2 mg of powder $CaCO_{3(s)}$ that is stored in a glass vial with a septum cap that is used for stable isotope analyses. After the collection, sets of 64 samples (one standard for each six powder samples) are analyzed in the Isotope Ratio Mass Spectrometer (IRMS), were the ratios of oxygen and carbon isotopes are measured by the analysis of carbon dioxide ($CO_{2(g)}$) resulted by the reaction of $CaCO_{3(s)}$ with $H_3PO_{4(l)}$ (concentration close to 100%) under controlled temperature at 72 ºC, from acid hydrolysis. The $CO_{2(g)}$ is carried to the Finnigan Gas Bench accessory by a $He_{(g)}$ flux and are separated from other gases by a gas chromatography system, and just after it is ionized and accelerated for separation by mass, with the whole procedure being semi-automatic.

The determination of the oxygen and carbon isotopic ratios is made through an ionic source in a triple collector of carbon and oxygen where the analytical results are based on the analyzes of nine sequential aliquots of each sample. The analytical precision is approximately 0.08 ‰ for the values of isotopic ratios of $^{13}C/^{12}C$ and ± 0.1 ‰ for the values of $^{18}O/^{16}O$ for samples with a minimum mass of 100 µg of $CaCO_{3(S)}$. The stable isotopic ratios are expressed using the notation δ defined by the difference between the ratio measured in the sample and the reference standard, divided by the reference standard ratio (Eq. 2). For the analyses, the international standard VPDB (Vienna Pee Dee Belemnite) was utilized, and the $\delta^{18}O$ and $\delta^{13}C$ values are expressed in per mil (‰). For this research, 1671 analysis were performed for the samples PIM-3, PIM-4 and PIM-5 and the resolution of each sample is presented in the following table:

Table 1 – Stalagmite samples analyzed for this study

Sample	Num. of analysis	Sampling resolution	Time-span (CE/BCE)
PIM3	160	0.2	1889-578 CE
PIM4	706	0.2	2013-338 CE
PIM5	805	0.4	587CE – 1020 BCE

3.3. Statistical Analyses

Since the U/Th method allows to obtain a well-resolved chronology for stalagmites and it grows continuously in time, the isotopic data obtained from the stalagmites can be displayed as time series with a discrete behavior of equal distance intervals from one point to the next. Since stalagmites present changes in the growth rates through time, a linear interpolation is made for each isotopic segment between two U/Th dating, which makes the final record a composite of all these temporal series. Thus, the analysis of speleothems' isotopic time series is used to determine several record attributes or behaviors such as periodicity or even to correlate with other time series from a different record or proxy.

For the periodicity analyses, REDFIT and Wavelet analyses are used here. Both methods require a record with an equal spaced time interval as input, so a new time series is generated using the interpolate/extrapolate tool from the software Origin with a two-year resolution (the record average resolution). The REDFIT is a function that obtains the spectral density of the data, averaging the spectra when splitting the time series into several segments and overlapping by 50%, reducing noise but also spectral resolution. This analysis yields the frequency by time spectra, which can be turned into periodicities when dividing the average time resolution of the record by the correspondent frequency (Hammer, 2019; Schulz & Mudelsee, 2018). The significance tests (from 95% to 99%) are made based on the chi2 method (Ghil et al., 2002) and when the power of determined frequency goes beyond these significance lines, that data is considered as a relevant periodicity for the record.

The wavelet transform verifies the record for occurrence and intensity of small, intermediate, and large scales periodicities (y axis) simultaneously over the given period (x axis). Once the y axis of this plot is a logarithmic size scale of base 2, the plot goes from more detailed view of the record on the top to a more smoothed general view towards the bottom. Also, a color scale is set to address the signal power or event intensity, going from more intense (red) to less intense (blue). The plot “cone of influence” is relevant to show where boundary effects are present (Hammer, 2019). Both REDFIT and Wavelet transform analysis were made using the software PAST. For the Wavelet transform, the lag was calculated using the ARMA with AR coefficients 0 and MA coefficients 1 (Hammer, 2019).

4. PUBLICATION

Patterns of paleoclimatic and paleoenvironmental changes in Amazonian lowlands over the last three millennia

M. E. Della Libera[1], V. F. Novello[1], F. W. Cruz[1], Vuille, M.[2], Orrison, R.[2], de Souza, J.[3], Maezumi S. Y.[4], Cauhy, J. R.[1], Campos, J. L.[1]; Ampuero, A[1].; Utida, G.[1]; Strikis, N. M.[5]; Edwards, R. L.[6]; Cheng, H.[6,7]

[1] Instituto de Geociências, Universidade de São Paulo, São Paulo, Brazil.
[2] Department of Atmospheric and Environmental Sciences, State University of New York at Albany, Albany, NY, USA.
[3] Department of Humanities, Universitat Pompeu Fabra, Barcelona, Spain.
[4] Institute for Biodiversity & Ecosystem Dynamics, University of Amsterdam, The Netherlands.
[5] Departamento de Geoquímica, Universidade Federal Fluminense, Niterói, Brazil.
[6] Department of Earth Sciences, University of Minnesota, Minneapolis, MN, USA.
[7] Institute of Global Environmental Change, Xi’an Jiaotong University, Xi’an, China

Corresponding author: Marcela E. Della Libera de Godoy (marcela.eduarda.godoy@usp.br)

Abstract

The paleoclimatic and paleoenvironmental history of the Amazon basin over the last millennia and the behavior of the South American Monsoon System (SAMS) throughout the lowlands have not yet been thoroughly examined due to a lack of records from more central portions of the basin. Here we discuss these past climatic changes based on new high-resolution $\delta^{18}O$ and $\delta^{13}C$ records from speleothems collected in the southwestern Amazon Basin, at the core region of the convective activity of the SAMS. We demonstrate that the $\delta^{18}O$ from these new records is representative of SAMS variations and that this convective system provides distinct precipitation patterns over the basin. The precipitation associated with SAMS is more homogeneously distributed over entire Amazon and Andes between 1000 BCE and 300 CE, whereas drier conditions prevailed over the western side of the basin during the Medieval Climate Anomaly (MCA, 950-1250 CE) and an east-west climatic dipole was established over the Amazon Basin after 1450 CE. The speleothem $\delta^{13}C$ record indicates an overall tendency toward a more humid tropical forest during the studied period, except for a drying during the MCA period. The paleoclimatic and environmental changes reported here seem to have been related to the dynamics of pre-Columbian cultures from southwestern Amazonia.

4.1. Introduction

The Amazon Basin holds the world's largest tropical forest and due to its broad extension and equatorial location, the forest is a major center of deep atmospheric convection, playing an important role in global climate regulation and atmospheric dynamics (Werth & Avissar, 2002). The Amazonian region accounts for much of the hydroclimate variability and rainfall balance over South America, with several of its large demographic centers relying on its moisture supply (Salati et al., 1979; Carvalho et al., 2002; Liebmann et al., 2004; Marengo et al., 2012; Carvalho and Dias, 2021). To thoroughly investigate and comprehend the past climate behavior of the basin is thus essential to understand its climate. It also results in a better understanding of how past climatic changes affected pre-Columbian populations; their cultures, migrations, and land-use systems (Iriarte et al., 2020; Souza et al., 2019; Maezumi et al., 2018), and allows putting projected future social, economic, and environmental impacts of climate change throughout South America in a long-term context (Iriarte, et al., 2020).

Records of past climate show evidence of distinct rainfall variations over the continent, related to changes in the South American Monsoon System (SAMS), which is the main climatic feature over the continent during austral summer-early autumn (JFM). These changes were likely related to changes in tropical Atlantic seas surface temperatures and regional atmospheric circulation (Zilli et al., 2019; Novello *et al.*, 2019; 2018; Vuille et al, 2012; Marengo et al., 2012; Cruz et al, 2009). Studies based on high-resolution stalagmite $\delta^{18}O$ records have investigated changes in SAMS activity, both over the last two millennia (e.g. Vuille et al, 2012; Thompson et al., 2013; Novello et al, 2018; Campos et al, 2019; Fig. 4.2-1) and on longer millennial- to orbital time scales (e.g. Cruz et al., 2009; Cheng et al., 2013b). These studies have identified a pervasive east-west precipitation dipole over South America due to changes in SAMS activity characterized by increased rainfall over the western Amazon and a consequent deficit recorded in Northeastern Brazil (NEB) and the eastern Amazon, or vice-versa. Moreover, Novello et al. (2018) explored the southwest-northeast shifts of the South Atlantic Convergence Zone (SACZ) during the past two millennia as evidence for changes in SAMS intensity, since the SACZ is a major monsoonal feature. Enhanced SAMS activity led to a southwestward displacement of the SACZ, thus facilitating the precipitation dipole (Novello et al. 2018; Campos et al., 2019).

Although of great relevance to the understanding of the SAMS, these records are either located far to the west in the Peruvian Andes (e.g. Bird et al. 2011; Thompson et al., 2013; Kanner et al., 2013), far to the east in NEB (e.g. Novello et al., 2012), or in central-western Brazil (e.g. Novello et al., 2018). Indeed, the past SAMS behavior over lowland Amazonia, which is located at the node of the South American climate dipole, is not well represented in the current paleoclimate archives. The only cave study that addresses paleoclimatic changes within the Amazon basin lowlands is based on a high-resolution paleoclimatic record from Paraíso cave (Wang et al., 2017). Nevertheless, the cave is situated in the northeastern Amazon basin (within the eastern domain of the climate dipole). Additionally, the study does not discuss late-Holocene climatic changes in depth, and relates the $\delta^{18}O$ differences between sites located in the eastern and western Amazon to the impact long-term vegetation changes had on the isotopic gradient across the basin. Therefore further investigation is needed to better understand the spatial variability of Amazonian paleoclimatic changes.

Based on the existing paleoclimate archives, important questions remain regarding the climate interpretation embedded in the speleothem isotope records, as well as the hydroclimatic linkages to changes in vegetation and natural or anthropogenic paleo-fire frequency during the past millennia, including: 1) What are the SAMS variability during the last three millennia in the area close to its core area in Southwestern Amazon? 2) Was the ant phasing between east and west across Amazonia, documented on orbital time-scales in the previous $\delta^{18}O$ records, also observed in the late Holocene? 3) How did pre-Columbian cultures respond to past climate changes in this region?

This study presents a new high-resolution speleothem record from a lowland region located in southwestern Brazilian Amazonia. We further employ an isotope-enabled climate model to analyze the history of environmental and climatic changes in Amazon and adjacent regions over the last 3 millennia. Our data is based on $\delta^{18}O$ and $\delta^{13}C$ analyses from stalagmites collected in a cave at the core of the SAMS domain filling an important gap along an east-west paleoclimatic transect across the Amazon and surrounding regions.

4.2. Samples, study site and modern climatology

The current study is based on two stalagmites (PIM4 and PIM5; Fig. 4.6-1) collected in Cuíca cave (11°40’S, 60°38’W, ~310 m a.s.l.) located in Pimenta Bueno city, Rondônia State, SW Amazon region in Brazil (Fig. 4.2-1). The stalagmites were collected in a chamber located ~200 m from the cave entrance, accessed by a narrow conduct upstream of the underground river that is eventually subject to flooding. Two temperature-relative humidity data loggers (TH1 and TH2; Fig. 4.6-2) were placed in distinct spots of the chamber over the course of one hydrological year (Sep. 2018 – July 2019) to monitor the temperature and relative humidity of the cave atmosphere. TH1 was placed on the wall close to the collected stalagmites and recorded a temperature ranging between 24.2 and 25.9°C; TH2 was located on top of the collapsed ceiling (~1.5 m below the current ceiling) and recorded temperatures between 24.4 and 24.8°C during this hydrologic year. Both devices registered 100% relative humidity during the monitored period. The cave site is located within the southwestern border of the Amazon Rainforest ecotone near the Cerrado (Brazilian savanna) biome. The area is close to the ecotone between Amazonian ombrophilous forest and the Brazilian savanna known as Cerrado (Miranda, 2000). Located within the core SAMS region, the nearby Pimenta Bueno city (11°40'S, 61°11'W, 60km away) rainy season is therefore mainly controlled by the monsoon regime, and the climate is characterized as tropical humid with an annual average temperature of 26°C. The average annual rainfall amount is about 1800 mm, over 90% of which falls between October and April during the summer monsoon season (Fig. 4.6-3).

The core SAMS region is defined by the unique shift in low-level (850 hPa) wind direction that occurs in the southwestern Amazon from easterlies (JJA) to westerlies (northwesterlies over the continent) during the monsoon period (Raia and Cavalcanti, 2008). The maximum influx of moisture from the tropical Atlantic occurs along the northern coast of South America and a more northerly trade wind component transports moisture southwestward into Amazonia, where strong convective activity takes place (Gan et al., 2004; Vera et al., 2006; Marengo et al., 2012; Vuille et al, 2012; Carvalho and Dias, 2020). The low-level moisture convergence over the monsoon exit region produces the SACZ, a key monsoonal feature characterized by persistent convection and an elongated zone of precipitation extending from the monsoon region southeastward across the continent into the subtropical Atlantic Ocean, providing significant amounts of moisture to central and southeastern Brazil (Carvalho et al., 2004; Marengo et al., 2012; Liebmann et al., 2004; Carvalho and Dias, 2020).

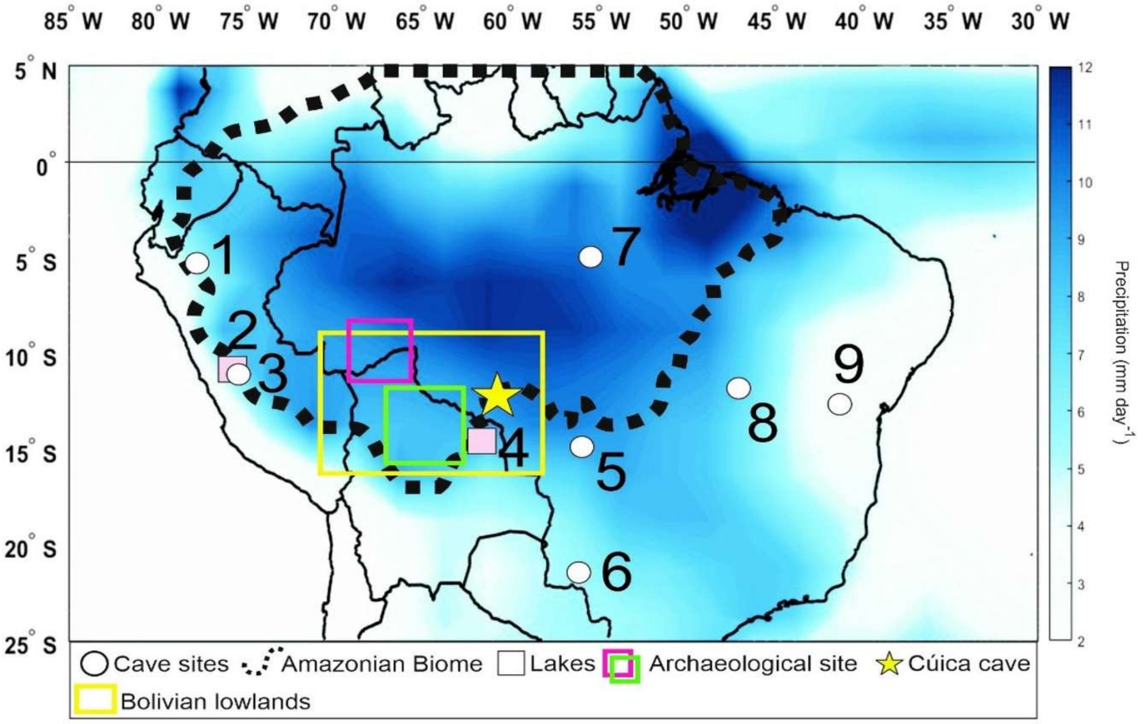

Figure 4.2-1 – Map of the South America with the locations of the records used in this study and the precipitation distribution in mm/day based on GPCP data during JFM, when SAMS is most active over the continent. Darker (lighter) blue indicates higher (lower) precipitation amount. The yellow star indicates the locatoin of our speleothems site in Rondônia state. The other sites are 1) Palestina cave (Apaéstegui et al., 2014); 2) Pumacocha lake (Bird et al., 2011); 3) Huaguapo cave (Kanner et al., 2013); 4) Laguna Chaplin (Maezumi et al., 2018); 5) Pau d'Alho and Curupira caves (Novello et al., 2016); 6) Jaraguá cave (Novello et al., 2018); 7) Paraíso cave (Wang et al., 2017); 8) Mata Virgem cave (Azevedo et al., 2019); 9) Diva de Maura cave (Novello et al., 2012). The yellow, green and pink squares demarcate the archeological regions named as the Bolivian lowlands (Maezumi et al., 2018), Llanos de Moxos and Southwestern Amazon (Souza et al., 2019), respectively.

4.3. Methods

4.3.1. Geochronology and composite

The geochronology of both PIM4 and PIM5, was established by means of the U/Th dating method by using an inductively coupled plasma-mass spectrometry (ICP-MS) technique at the Geochronology Laboratory at the University of Minnesota (USA) and at the Institute of Global Environmental Change, Xi'an Jiaotong University (China), following the methodology described by Cheng et al. (2013a). The $\delta^{18}O$ and $\delta^{13}C$ analyses were performed at the Stable Isotope Laboratory at the Institute of Geoscience of the University of Sao Paulo using a Thermo-Finnigan Delta Plus Advantage mass spectrometer coupled to a Gas-Bench system. The notation δ in the results refers to the relative Vienna Pee Dee Belemnite standard (VPDB) with the per mil deviation, and its reproducibility is 0.1‰ for both analyses.

Initially, the isotopic series were linearly interpolated between the ages to generate the geochronological models for the isotopic records. We use a 1000 Monte-Carlo simulation approach to produce age-depth models to merge the two $\delta^{18}O$ stalagmite records by accounting for 1σ error age uncertainties and also to interpolate the isotopic data. The two $\delta^{18}O$ records were merged through normalization (i.e., by subtracting the mean and dividing by the standard deviation) of the data inside the overlapping period, averaging both series and then reconstructing the shorter time series with the mean and standard deviation of the longer one, for each interpolated isotope time series (Monte-Carlo simulation).

4.3.2. Model analysis

Data from the Community Earth System Model isotope-enabled Last Millennium Ensemble (CESM-iLME) project is used to interpret the dynamical controls on $\delta^{18}O$ at the location of the PIM4 record. CESM is a fully-coupled state of the art climate model with an approximate one degree horizontal grid spacing. The model was run with transient forcings from reconstructions covering the period 850-1850 CE, replicating the experiments conducted for the non-isotope enabled model experiments (Otto-Bliesner et al., 2016). This analysis is based on composites of three ensemble members forced by the full suite of external forcings to examine the dynamics of the rainy season (January, February, and March) during periods of enrichment and depletion of ^{18}O in precipitation within the model environment. A precipitation-weighted $\delta^{18}O_{precip}$ ($\delta^{18}O$ from precipitation) time series was constructed for seasonal anomalies of each ensemble member. Due to the spatial uniformity of the $\delta^{18}O_{precip}$ signal and to average out some internal variability of the single point location, the analyzed time series is derived from a 3x3 grid area centered on the location of Cuíca cave. Composites were established based on exceedance of a +/- 2 sigma threshold by the anomaly time series relative to a given ensemble member mean, and the results were then averaged. In addition to $\delta^{18}O_{precip}$, mid-tropospheric vertical velocity (omega values at 524 hPa, negative values indicating upward motion) and precipitation fields were analyzed for the composited seasons. The statistical significance was tested for composites using a two-tailed student's t-test ($p < 0.05$) for each ensemble member, and grid cells are indicated where at least 90% of composited seasons are statistically significant. Statistical significance for difference plots between composites of precipitation that is depleted and enriched in ^{18}O isotopes was based on the total composite member differences.

4.4. Results

The speleothem PIM4 is a12 cm tall stalagmite and spans the period between 338-2013 CE (Fig. 4.4-1). Its isotopic profile is composed by 706 $\delta^{18}O$ and $\delta^{13}C$ analyses and yields an average temporal resolution of 2.4-years. According to the roughly uniform distribution of the 21 U/Th ages along the stalagmite (errors <1%), a short 100-year hiatus is evident (1046-1146 CE), and there is no evidence of long hiatuses. The segment used from PIM5 (34 cm long) spans from 1020 BCE to 587 CE with chronology based on 16 well-distributed U/Th ages (Fig. 4.4-1). It overlaps with PIM4 by a 200 years interval. PIM5 isotopic profile is composed of 805 isotopic analyses with a 2-year resolution on average. Therefore, since both samples share a similar range of $\delta^{18}O$ values during the overlapping period, combining the two samples provides a composite record of the last 3000 years from southwest Amazon basin, based on 37 U/Th ages with an average record resolution of 2 years.

The Cuíca cave $\delta^{18}O$ composite record presents values ranging between -5.1 and -7.4‰ with a mean value of -6.6‰ (Fig. 4.4-1). From 1020 BCE until 270 CE the $\delta^{18}O$ values present a mean of -6.82‰, with a range of variability of ~0.6‰ and absence of an isotopic trend; between 270-850 CE the values increase until they reach a maximum value of -5.1‰ at about 850 CE. From 850 CE to 1800 CE a general trend towards more negative values prevails, yet two negative excursions occur centered at 1260 CE (-6.7 ‰) and ~1740 CE (-7.1‰), which are separated by a positive excursion centered at 1370 CE (-5.5‰). From 1800 CE to the present, the $\delta^{18}O$ values continue with a multidecadal variability around the mean of -6.7‰, similar to the period before 850 CE.

The $\delta^{13}C$ record is characterized by a negative isotopic trend extending from its oldest portion until ~100 CE, dropping from its highest value (-9.2‰) centered at ~980 CE to its lowest value centered at 170 CE, superimposed on centennial variability with an amplitude of 1.2‰, whereas the $\delta^{18}O$ is rather stable during this period (Fig. 4.4-1). From 170 CE until 1800 CE the $\delta^{13}C$ record displays trends which are consistent with those seen in the $\delta^{18}O$ record, but with reduced variability at decadal to centennial time scales. From 1800 CE onwards, the $\delta^{13}C$ trend differs from $\delta^{18}O$, continuing its decreasing trend until the present.

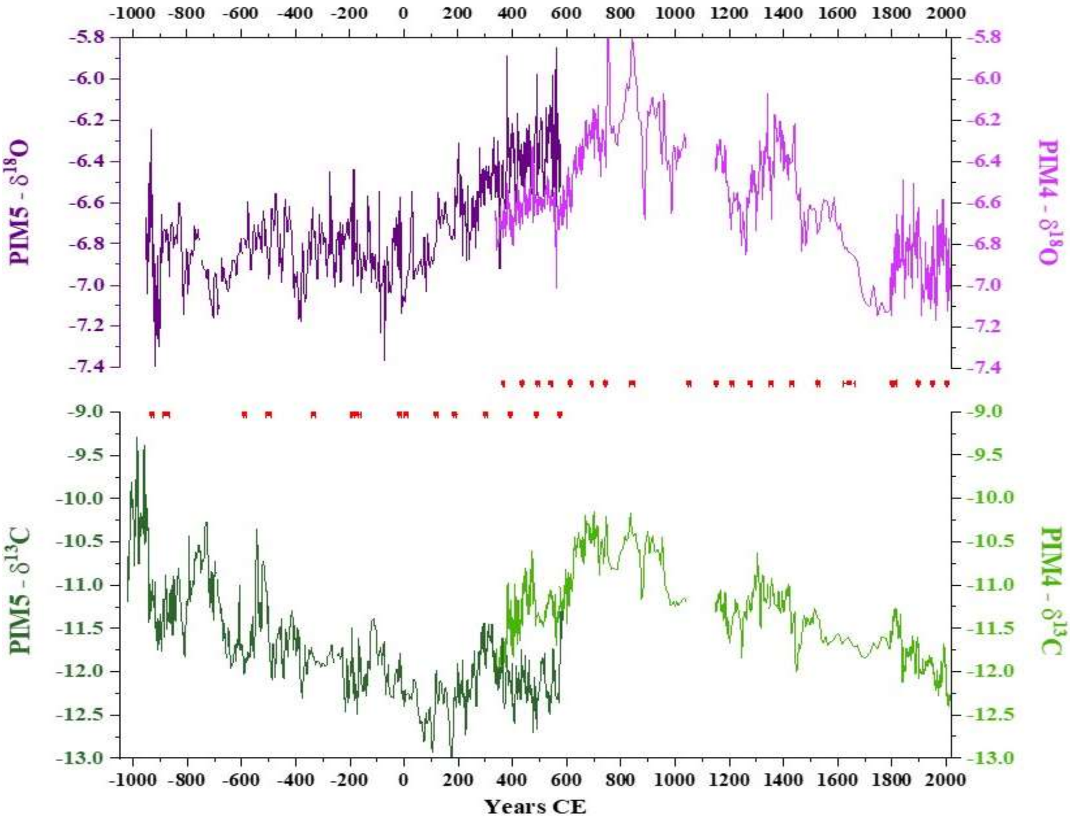

Figure 4.4-1 - (top) $\delta^{18}O$ time-series obtained from the stalagmites PIM4 (light purple) and PIM5 (dark purple). (bottom) $\delta^{13}C$ time-series obtained from the stalagmites PIM4 (light green) and PIM5 (dark green). U/Th dates and their corresponding error bars are shown in red between $\delta^{18}O$ and $\delta^{13}C$ records.

4.5. Discussion

4.5.1. $\delta^{18}O$ data interpretation

In this section, we discuss the modern climate data based on the rainfall monitoring station installed near the cave site (Pimenta Bueno city), from where almost one year of precipitation amount and rain water $\delta^{18}O$ and δD data were collected (Sep 2018 – July 2019), and the CESM-iLME climate model. Considering we have the equivalent of only one hydrologic cycle from our rainfall monitoring station at the cave site, observational data from the Global Network of Isotopes in Precipitation (GNIP) of the two nearest meteorologic stations, Porto Velho (400km) and Cuiabá (600km), are here used to assist on the interpretation of the $\delta^{18}O$precip isotopic signature given they are located within the same climatic context.

The rain water $\delta^{18}O$ and δD collected weekly at the cave site, along with the isotopic data obtained from cave drip water collected during fieldwork, plot on top of the global meteoric water line (GMWL) (Fig. 4.5.1-1a), demonstrating that the isotopic signal is not significantly affected by the seepage through the epikarst and thus indicating the speleothems' potential to reconstruct the local paleoprecipitation. In addition, the minor temperature variations recorded inside the cave throughout the year and the relative humidity always under saturated conditions favor calcite precipitation close to isotopic equilibrium, with little kinetic effects that could lead to isotopic fractionation, therefore preserving the original isotopic signal from precipitation during calcite deposition and speleothem formation. This is demonstrated by the isotopic values of modern calcite precipitated on watch glasses placed underneath three dripping sites in Cuíca cave (Fig. 4.6-4), which are within the predicted $\delta^{18}O$ values for carbonate deposited in approximate equilibrium conditions with drip water according to the cave average temperature of 25°C (Johnston et al., 2013). Thus, the environmental conditions in which the speleothems are formed in Cuíca cave are ideal for preserving the climatic signal embedded in the oxygen isotopes of the rainwater.

Regarding the processes that affect and control $\delta^{18}O_{precip}$ isotopic signature, both amount effect and degree of rainout upstream (DRU) are considered here. The comparison between the weekly, biweekly and monthly accumulated amounts and the rainfall $\delta^{18}O$ show significant negative correlations (r = -0.41, -0.55, -0.64, respectively – Fig. 4.5.1-1b), demonstrating that the rainfall amount is a very relevant factor on the $\delta^{18}O_{precip}$ composition at Cuíca cave site at these timescales. Besides, the degree of rainout along the northeasterlies trade winds results in a further isotopic depletion in ^{18}O during water vapor transport from tropical Atlantic ocean across Amazon (Salati et al., 1979; Vuille et al., 2012; Ampuero et al., 2020). The comparison of the monthly precipitated amount data at our local monitoring station, very close to Cuíca cave, with the monthly average precipitation at Pimenta Bueno ANA (Agência Nacional de Águas) rainfall monitoring station, and Porto Velho and Cuiabá GNIP stations (Fig. 4.5.1-2a), reveals the consistent spatial and temporal variations in $\delta^{18}O_{precip}$ associated with SAMS. These stations show similar $\delta^{18}O_{precip}$ variability, despite of differences in annual mean rainfall that decrease southward to Cuiabá with increasing in distance from the monsoon core region. Yet, the monthly precipitation-weighted $\delta^{18}O_{precip}$ at Porto Velho, Cuiabá and our monitoring site (Fig. 4.5.1-2b) present the same isotopic signature trend throughout the year, and all three sites show a significant negative correlation (r= -0.86, -0.77, -0.64, respectively) between precipitation amount and $\delta^{18}O_{precip}$ (Fig. 4.5.1-2c), where months with higher (lower) rainfall amounts are the summer (winter) months, thus demonstrating the effect of DRU through Rayleigh distillation during the SAMS season. Finally, considering over 90% of the annual rainfall amount occurs during the monsoon season (October-April), precipitation during the winter months plays a negligible role in the stalagmite isotopic composition, what enables the stalagmites' interpretation as a proxy for the rainfall associated with the SAMS.

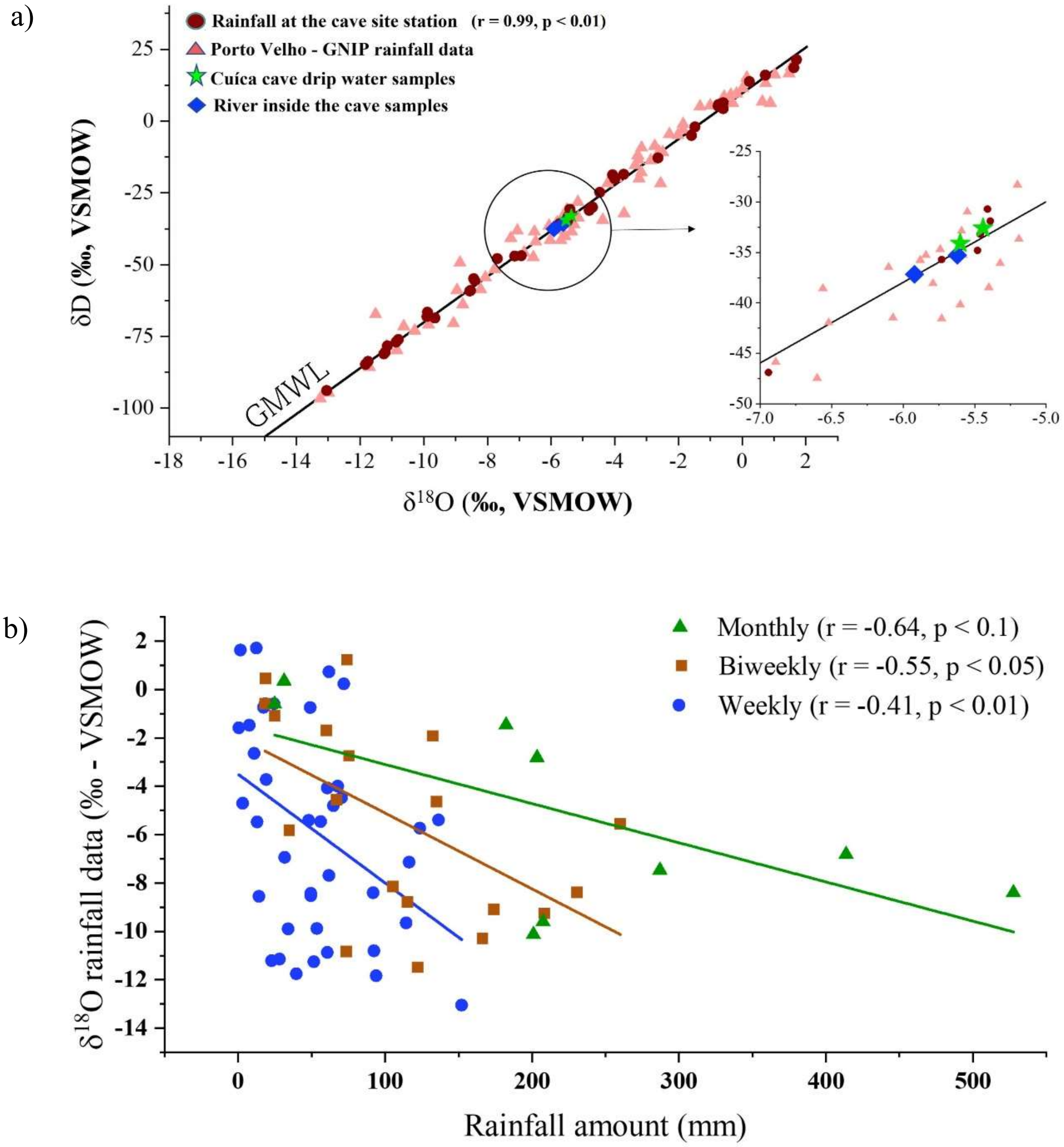

Figure 4.5.1-1 - a) $\delta^{18}O$ and δD (‰, VSMOW) values of: rainwater samples collected at Cuíca cave site (red dots); rainwater from the GNIP database from Porto Velho (pink triangles); samples from Cuíca cave drip water (green stars); water sample from the river running inside Cuíca cave (blue diamonds). All data are plotted on top of the Global Meteoric Water Line (GMWL).

In addition, composite analyses using the CESM model with complete transient forcings over the last millennium documents the regional dynamical patterns associated with periods of strong depletion and enrichment in ^{18}O of the rainwater precipitating at Cuíca cave (Fig. 4.5.1-3). The composite analysis shows that precipitation depleted (enriched) in ^{18}O corresponds to enhanced (reduced) upward motion over equatorial South America upstream of the cave site (Fig. 4.5.1-3,a,b). The precipitation anomalies are largely co-located with regions of vertical motion anomalies, with rising motion triggering convective precipitation (Fig. 4.5.1-3d) and subsidence suppressing precipitation (Fig. 4.5.1-3e). Difference plots (Fig. 4.5.1-3c, f, i) highlight that while there is some correspondence between local changes in $\delta^{18}O_{precip}$ and co-located convection, the upstream activity dominates over the magnitude of local controls on isotopic extremes.

Considering what was presented above, we interpret changes in the $\delta^{18}O$ record from Cuíca cave to be driven by the amount effect on local rainfall isotopic composition and also the precipitation that occurred along the moisture trajectory from the Atlantic to the site by DRU factor. Yet, local precipitation and, therefore, amount effect are related to SAMS intensity, thus an enhanced (weakened) SAMS activity leads to more depleted (enriched) $\delta^{18}O$ values by both DRU and amount effect processes.

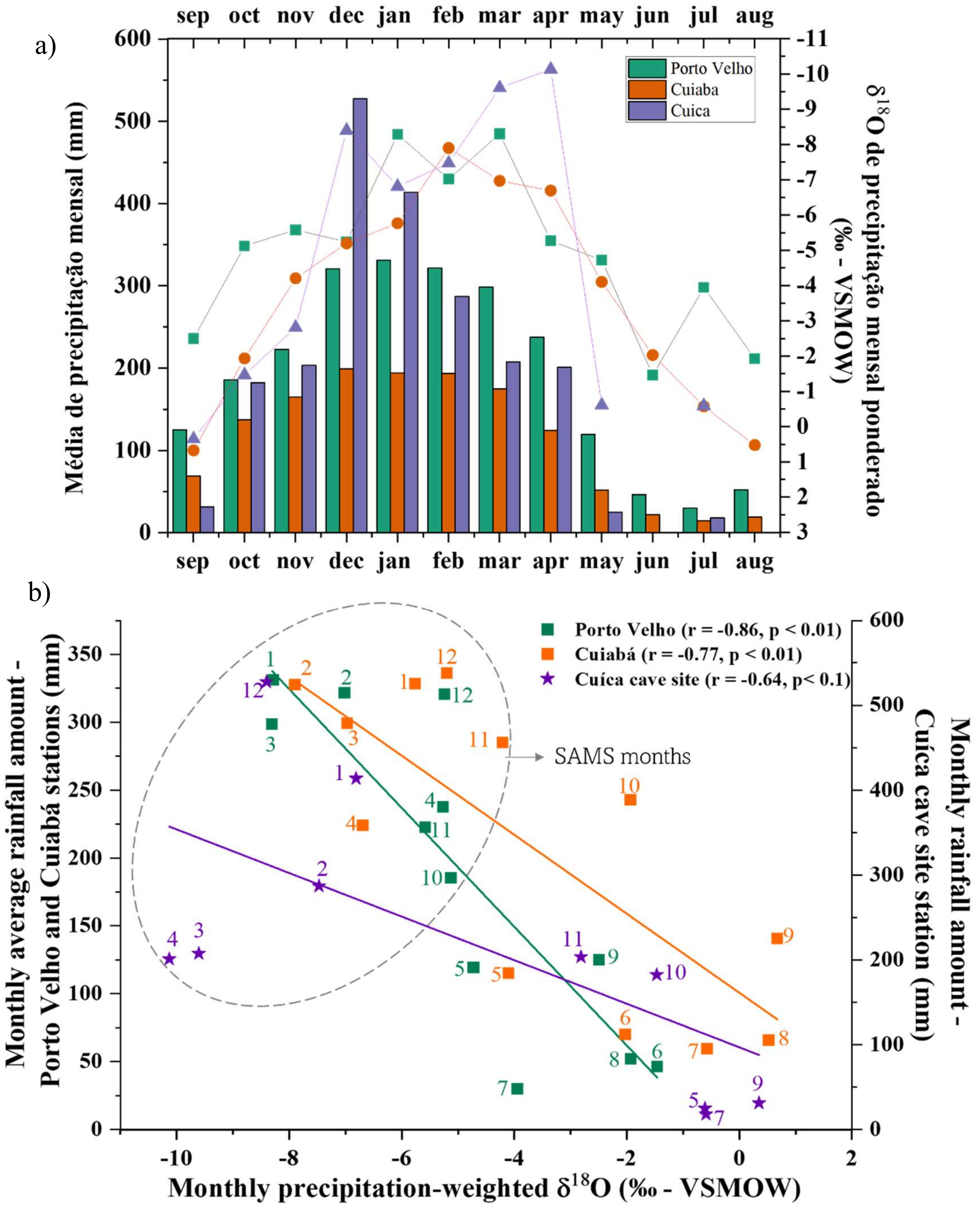

Figure 4.5.1-2 – a) Comparison between the monthly accumulated rainfall at the monitoring station at Cuíca cave site from Sep 2018-July 2019 (purple bar), the monthly average precipitation at Porto Velho (green bar), and Cuiabá (orange bar) cities, with monthly precipitation-weighted $\delta^{18}O$ at the Cuíca cave site (purple triangle), and Porto Velho (green square) and Cuiabá (orange circle) GNIP stations from 1965-1980. b) Monthly precipitation-weighted $\delta^{18}O$ vs.

monthly average precipitation amount from Porto Velho and Cuiabá, and monthly accumulated rainfall at Cuíca cave site. The numbers indicate the months.

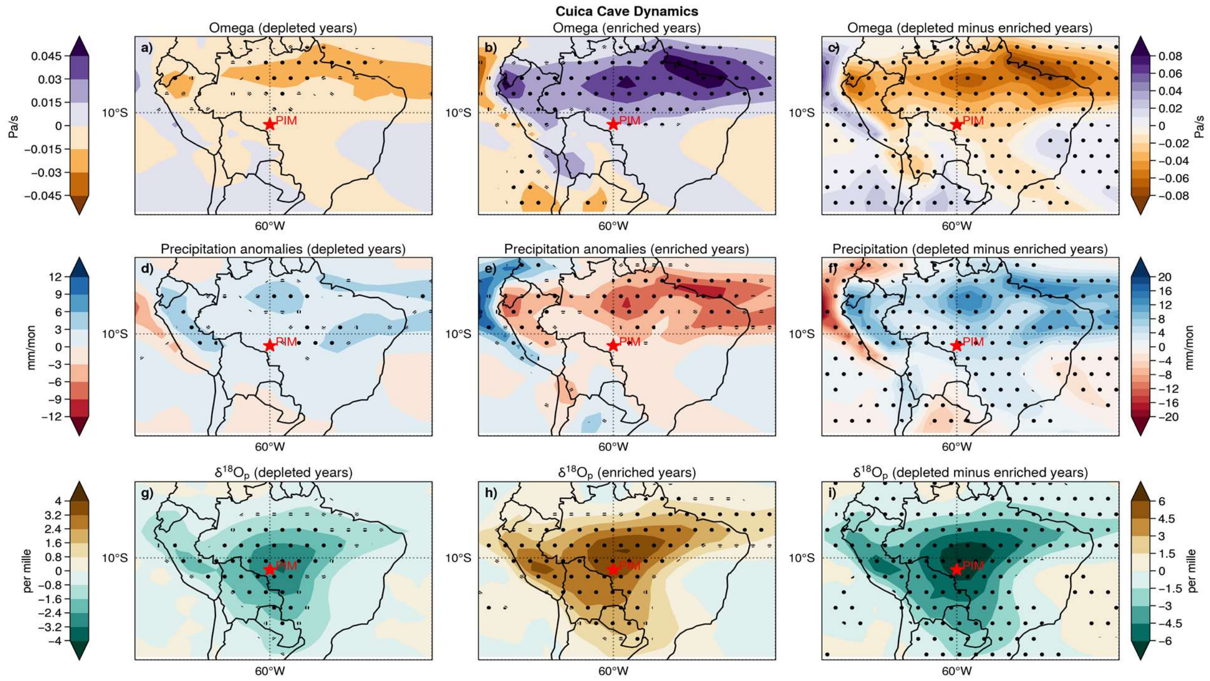

Figure 4.5.1-3 - Composite analysis of Cuíca cave dynamics using CESM-iLME full forcing experiment. Stippling in columns 1 and 2 represent grid cells where 90% of composite members are statistically significant for depleted (n=30 members) and enriched (n=123 members) composites, respectively. Stippling in column 3 represents statistically significant differences at $p<0.05$. Row 1 show results for mid-tropospheric vertical motion (negative indicating upward motion) at 524 hPa; row 2 shows results for precipitation, and row 3 shows results for $\delta^{18}O_{precip}$. Cuíca cave location is indicated with a red star in all plots.

4.5.2. $\delta^{13}C$ data interpretation

Several processes can affect the $\delta^{13}C$ record in stalagmites, including: vegetation type and density above the cave, temperature, fractionation due to in-cave atmospheric conditions and prior calcite precipitation (PCP) related with local hydrological conditions. This hampers the interpretation of $\delta^{13}C$ records in stalagmites, since it cannot be attributed to a single process or climatic signal. However, variations in $\delta^{13}C$ from a collection of stalagmites collected at different locations across tropical South America have been attributed to PCP, with positive feedbacks related to changes in vegetation as the main control on $\delta^{13}C$ values of these stalagmites (Novello et al., 2021). PCP increases during drier periods due to the longer exposure of the seepage solution to air that promotes significant calcite precipitation in the vadose zone while forming the stalagmites with higher $\delta^{13}C$ values in the cave galleries (Fairchild & Baker, 2012; Fohlmeister et al., 2020). In comparison, local wet conditions favor C_3 over C_4 plants, increase biogenic CO_2

production by enhancing soil respiration rates and inhibit PCP in the epikarst, all contributing to more depleted $\delta^{13}C$ values in the stalagmites (Novello et al., 2021 and references therein).

These processes controlling $\delta^{13}C$ values in stalagmites also contributes to a positive correlation between $\delta^{13}C$ and $\delta^{18}O$ in stalagmites located in monsoonal regions where the SAMS is the main provider of moisture and the main control on $\delta^{18}O$ variability, thus local precipitation amounts and convective processes are closely related (Novello et al., 2021), which is the case of the study area. Cuíca cave is located inside of the broad region studied by Novello et al. (2021), sharing the same characteristics as the other caves in western Amazonia/central-west Brazil regions, such as a constant cave atmosphere, shielded against external atmospheric fluctuations, thereby avoiding major impact by kinetic fractionation processes inside the cave (see Section 2). Furthermore the Amazon region was not subjected to extensive changes in temperature through the last three millennia, avoiding significant temperature effects on the $\delta^{13}C$ values of the stalagmites (Van Breukelen et al., 2008). All these factors indicate that the $\delta^{13}C$ from Cuíca cave may reflect local moisture conditions and soil/vegetation dynamics.

4.5.3. Paleoclimate dynamics over Amazon Basin

The Cuíca $\delta^{18}O$ record documents the weakest SAMS activity between 700 and 1200 CE, and the strongest activity between 1400 and 1800 CE. Overall, this is in accordance with other $\delta^{18}O$ records from western South America, such as Jaraguá cave (Novello et al., 2018) in southwestern Brazil (21°S/56°W), Pau D'Alho cave (Novello et al., 2016) in central-west Brazil (15°S/56°W), Huagapo cave (Kanner et al., 2013) and Pumacocha lake (Bird et al., 2011) in southern Peru (11°S/75°W), and Palestina cave (Apaéstegui et al., 2014) in northern Peru (5°S/77°W) (Fig. 4.5.3-1).

A development towards a drier climate emerges after 620 CE in the Cuíca record, indicating a progressively weakening of SAMS until 850 CE during the MCA period, when the monsoon regime reaches its weakest intensity observed in the last 3 kys. This general dry scenario during the MCA is also seen in the western Brazil records such as Jaraguá and Pau d'Alho caves, located to the west of the mean SACZ position. They display anomalously positive values at this time, likely indicating a decrease in moisture flux over the SAMS/SACZ domain (Fig. 4.5.3-1). Less negative $\delta^{18}O$ values during the MCA are particularly evident in the Peruvian records of Pumacocha lake, and Palestina and Huagapo caves, all located along the western margin of the

SAMS domain. It is noteworthy, however, that the largest excursions of $\delta^{18}O$ to higher values in these western SAMS records are not synchronous during the MCA, which is possibly because these records located on the eastern Andes flank and thus are also affected by the Pacific ocean fluctuations (Bird et al., 2011; Kanner et al., 2013; Apaéstegui et al., 2014). Following the MCA, the time period between 1260 and 1450 CE, is also marked by an anomalous dry period in the Cuíca record, although not as strong as during the MCA. This anomaly is also observed in some of the other western Amazon records, such as Huagapo, Pumacocha and Jaraguá, all showing above-average $\delta^{18}O$ values during this period (Fig. 4.5.3-1).

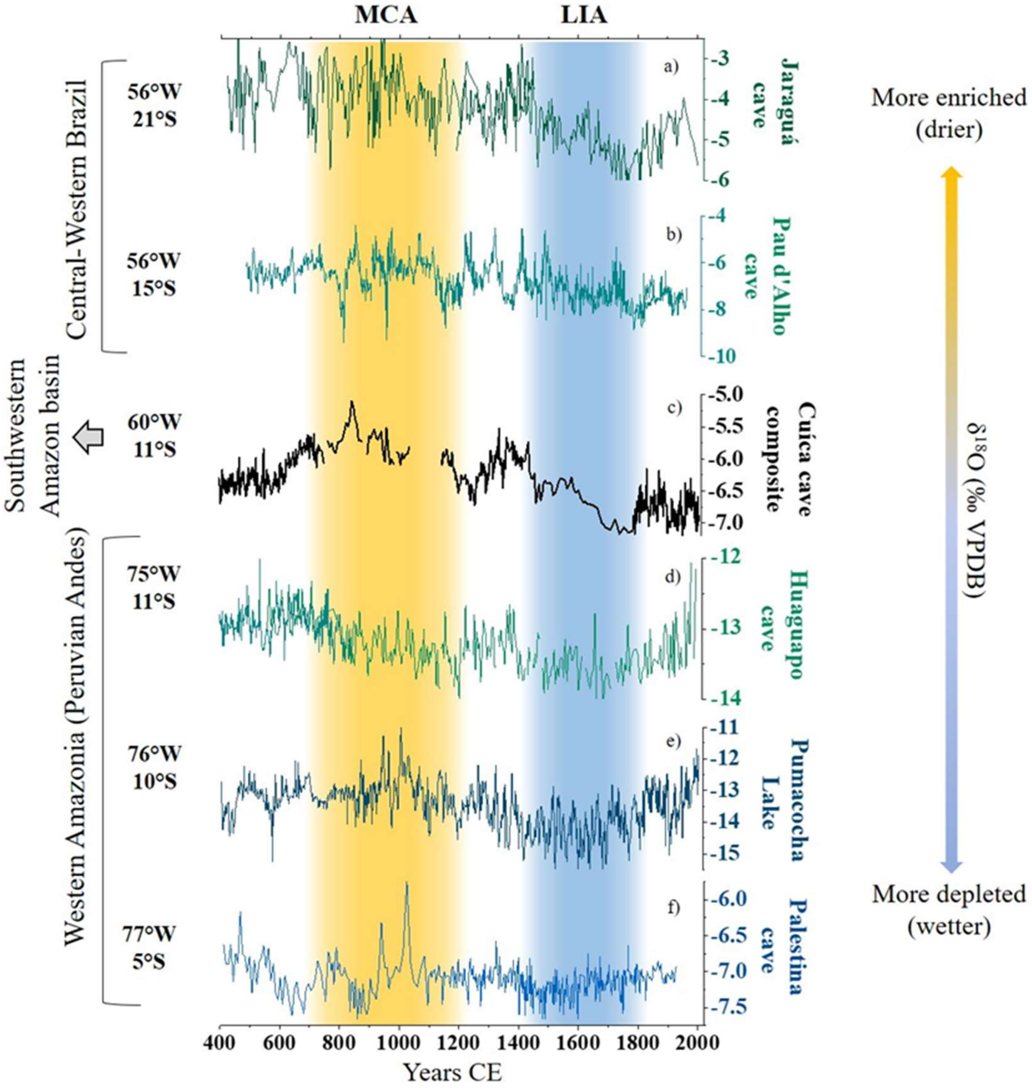

Figure 4.5.3-1 - Comparison between the δ18O records from western/southwestern Amazonia and Central-West Brazil. They are: a) Jaraguá cave (Novello et al., 2018) and b) Pau d'Alho cave (Novello et al., 2016) in central-western Brazil; c) Cuíca cave composite (this study) in Southwestern Amazon basin; d) Huaguapo cave (Kanner et al., 2013),

e) Pumacocha lake (Bird et al., 2011) and f) Palestiva cave (Apaéstegui et al., 2014) in the Peruvian Andes (western Amazon).

In contrast, the following period (1450-1800 CE) corresponding to the Little Ice Age (LIA) (Vuille et al., 2012; Novello et al., 2018) is marked by enhanced SAMS activity, at the Cuíca site. This is the time window during the last 3000 years where most of the paleoclimate records from western South America and central-west Brazil are synchronized (Fig. 4.5.3-1). At the beginning of the LIA period, the Cuíca $\delta^{18}O$ record drops by 1‰, resulting in values that are 2‰ more negative than the highest values of the MCA period. Given that Cuíca cave is located within the core region of SASM convective activity, this shift in the mean state towards a wetter LIA indicates a strengthening of the monsoon over a large portion of the South American continent, affecting the isotopic composition of cave records from the northern Peruvian Andes to central-western Brazil (Bird et al., 2011; Vuille et al., 2012; Kanner et al., 2013; Novello et al., 2016; 2018; Campos et al. 2019).

The drier-MCA and wetter-LIA framework presented here is, however, not true for tropical South America as a whole, but only for the regions discussed this far (Vuille et al., 2012; Novello et al., 2012; Campos et al., 2019; Azevedo et al., 2019). To illustrate the distinct climatic variability over tropical South America during these periods, we compare speleothem $\delta^{18}O$ records from western Amazon (Pumacocha lake and Cuíca cave) with eastern Amazon/Brazil Nordeste (Paraíso and Mata Virgem cave, and Diva de Maura cave, respectively) (Fig. 4.5.3-2). The most distinct feature among all these records is the anti-phasing between wet conditions at Pumacocha and Cuíca, and the drier scenario over the eastern Amazon and SAMS branch (Paraíso, Mata Virgem and Diva de Maura) during the LIA period.

Even though this dipole feature has been previously documented based on records in the Peruvian Andes and NEB (Thompson et al., 2013; Novello et al., 2018), here we introduce the Cuíca record to this discussion to assess this dynamic from the perspective of the core monsoon domain in the southwestern Amazon. In addition, we analyze the $\delta^{18}O$-gradient between the Cuíca and Diva de Maura caves, located over the western and eastern poles of the climate dipole, respectively (Fig. 4.5.3-3), in the CESM-iLME model. These results indicate that intensified upward motion and convection over the Cuíca cave region (southwestern Amazon) is associated with enhanced subsidence over NEB and the Diva de Maura cave, resulting from an intensified upper-tropospheric wave guide, known as Bolivian High-Northeast Low system, and a contemporaneous southwesterly displacement of the SACZ (Novello et al., 2018). Hence, the enhanced $\delta^{18}O$ gradient between both sites reflects the surface expression of a dynamic, atmospherically-induced dipole pattern that can be observed in the isotopic proxy data during the LIA and is reproduced in the iCESM model at times when the simulated $\delta^{18}O$ at the Cuíca cave reach their most negative value. Also, it is likely that the extended subsidence over NEB branch affects the Mata Virgem region further to the west of Diva de Maura at 47°W, as well as Paraíso region on north-eastern Amazon at 55°W/4°S, in addition to a southwestward SACZ displacement (Novello et al., 2018). However, the largest changes seen in both mid-tropospheric vertical motion and precipitation are located upstream of the Cuíca site, suggesting that the local isotopic signal is reflective of larger-scale upstream circulation changes, rather than only local conditions, indicating an overall enhanced monsoon activity. Therefore, this striking anti-phased behavior during LIA displays the clearest stage of an east-west precipitation dipole over the Amazon region until present days.

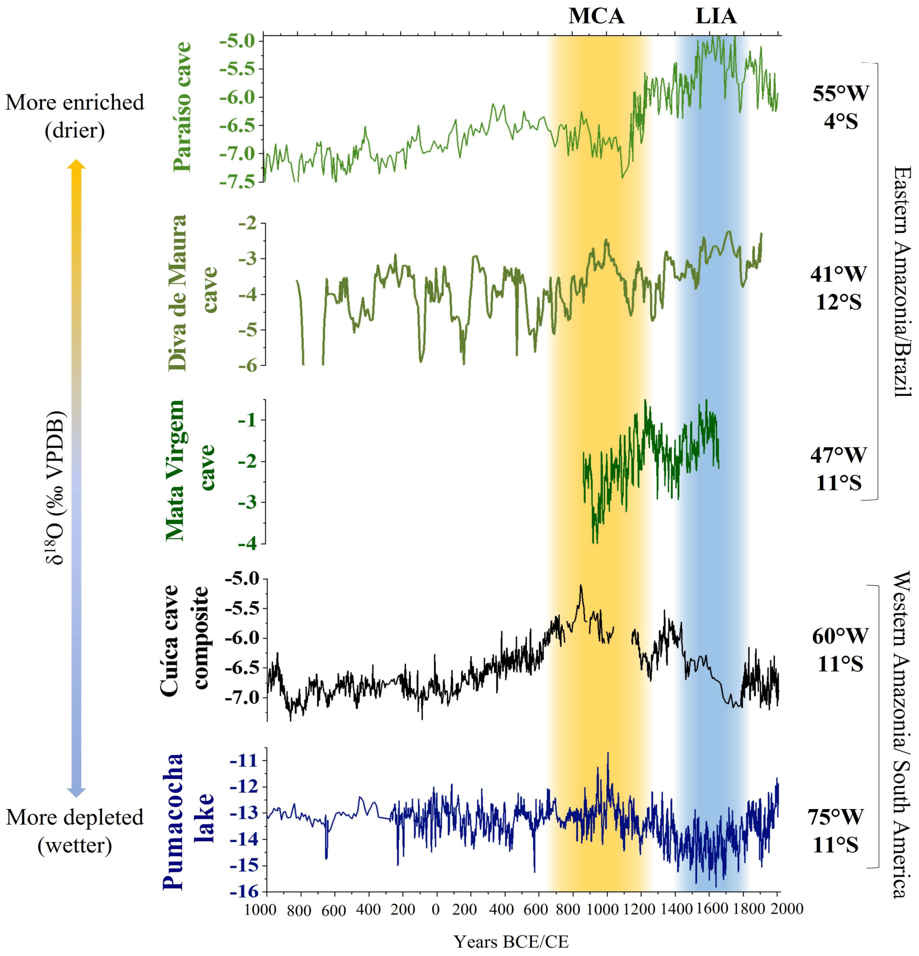

Figure 4.5.3-2 - Comparison between the $\delta^{18}O$ records at opposite Amazon basin sides that display the east-west precipitation dipole. The sites are: a) Paraío cave (Wang et al., 2017); b) Diva de Maura cave (Novello et al., 2012); c) Mata Virgem cave (Azevedo et al., 2019); d) Cuíca cave composite (this study); e) Pumacocha lake (Bird et al., 2011).

On the other hand, drier conditions over the core of monsoon (Cuíca and Pumacocha) during MCA are also evident in NEB (Diva de Maura) (Fig. 4.5.3-2), what is coherent with a lower moisture income from tropical Atlantic ocean since it plays a major role in moisture supply for both regions (Novello et al., 2012; Marengo et al., 2012), whereas Paraíso and Mata Virgem records present a wet stage (Azevedo et al., 2019). Albeit these three regions are under major influence of SAMS activity, humidity from north-eastern Amazon (Paraíso cave region) may have been transported over Mata Virgem cave region, thus sustaining a wet phase during a weakened SAMS activity (Azevedo et al., 2019).

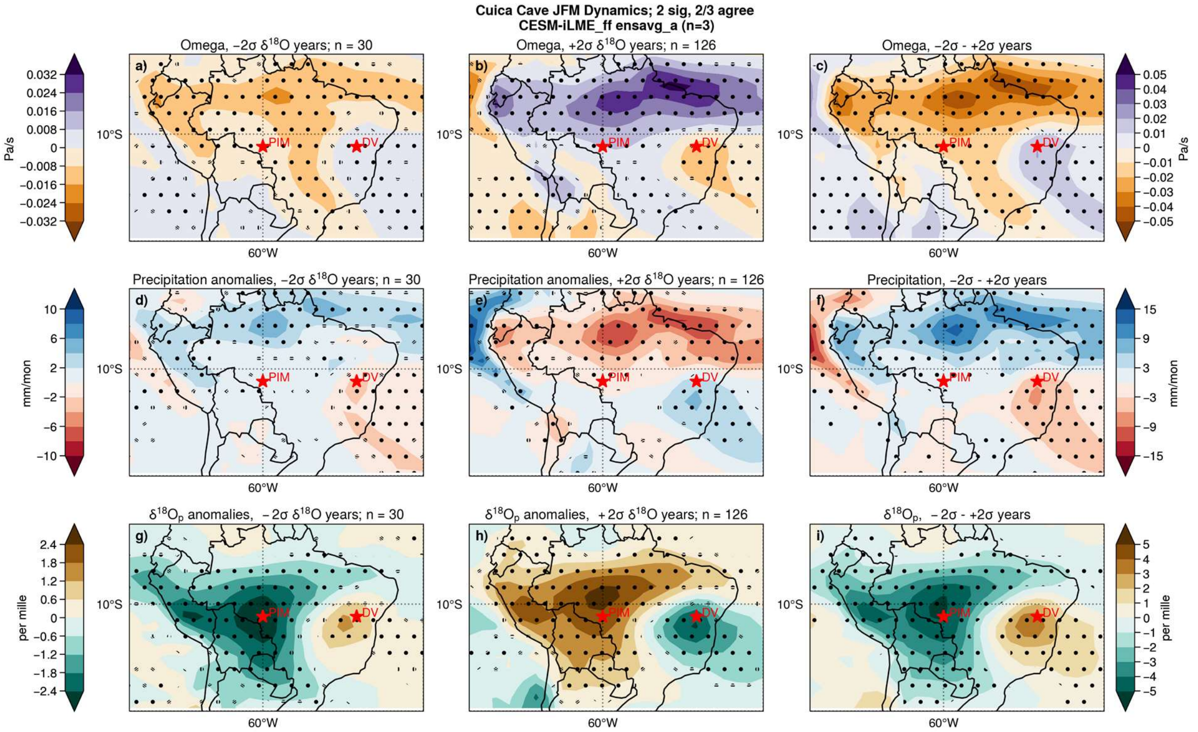

Figure 4.5.3-3 - CESM-iLME $\delta^{18}O$ gradient model plot with 67% level of agreement between Cuíca cave (red star on the left identified as PIM) and Diva de Maura cave (red star on the right identified as DV; Novello et al., 2012) for vertical motion (omega) at 524hPa (Pa/s; a,b,c), precipitation (mm/mon; d,e,f) and $\delta^{18}O$ (per mil; g,h,i). Composites were built from selected seasons in which the local $\delta^{18}O_{precip}$ time series exceeded +/- 2 standard deviations (sigma) of a given ensemble member mean for the period of interest. The negative (a,d,g) and positive (b,e,h) two sigma composites are the groupings of seasons that have the greatest and weakest $\delta^{18}O$ gradient between the two cave sites, respectively. Plots c, f and i show the difference plot between the sigma plots (negative-positive).

4.5.4. Paleoenvironmental changes in southwestern Amazonia and archeological implications

The decrease of the $\delta^{13}C$ values in the Cuíca record from 1000 BCE to 200 CE occurs without significant changes in the SAMS documented by the $\delta^{18}O$ record (Fig. 4.5.4-1). This is attributed to a progressive increase in vegetation density across the region, driven by a southward migration of the rainforest-savanna ecotone (Mayle et al. 2000; Burbridge et al. 2004). This southern expansion of rainforest vegetation is characterized by an increase in C_3 plant density over C_4 plants, as is documented by the increase in Moraceae from 6 to 20% and decrease of Herbs from 55 to 35% in the pollen record from Laguna Chaplin (LCH) (Fig. 4.5.4-1) in northern Bolivia (14ºS/61°W; Maezumi et al., 2018), 300 km south of Cuíca cave (Fig. 4.2-1). Burbridge et al. (2004) also document an increase in Moraceae in Laguna Bella Vista (200 km south of Cuíca cave) during the same period, which corroborates this interpretation. This is consistent with many paleovegetation reconstructions from the Amazon that documented a gradual southward expansion of humid tropical forest and a retraction of the seasonally dry tropical forest since the mid-Holocene (Smith and Mayle, 2018; Mayle and Power, 2008; Haberle and Maslin, 1999; Taylor et al., 2010).

During MCA period, the ~2‰ increase of $\delta^{13}C$ values in Cuíca cave and the ~10% decrease of Moraceae in LCH point to a vegetation retraction due to the weak SAMS as documented by the Cuíca $\delta^{18}O$ record (Fig. 4.5.4-1). The high $\delta^{13}C$ values in Cuíca during the MCA period are reinforced by the increase of the PCP due to low water availability at the cave epikarst. After the MCA, a progressive trend toward more negative Cuíca $\delta^{13}C$ values until the present indicates a vegetation expansion associated with more humid conditions. During this period, there is an abrupt increase of % Moraceae and a decrease % Herbs in LCH, and for the first time in the last 3000 years the % Moraceae overcome % Herb, which points to an ecotonal expansion of humid tropical forest that replaces seasonally dry forest and savanna swamps. This vegetation change is also corroborated by the Laguna Bella Vista pollen record (Mayle et al., 2000; Burbridge et al., 2004; Maezumi et al., 2018). These abrupt changes in vegetation also occurred during the period when the SAMS intensified (as documented by the Cuíca $\delta^{18}O$ values during the LIA). These data indicate a close relationship between SAMS intensity and vegetation changes in the region during the last millennium, as already proposed by Novello et al. (2021) for tropical South America.

To assess the relationship between environment and climate changes with the dynamics of pre-Columbian cultures we compare the Cuíca isotopic records with previously published regional archeological data (Maezumi et al. 2018; de Souza et al. 2019) using the sum of the calibrated probability distribution (SPD) as an estimate of past populations dynamics based on the density of ^{14}C ages in archeological sites. Maezumi et al. (2018) compiled AMS-dates of the relationship between palaeofires and archeological sites from the Bolivian lowlands, which includes the location of Cuíca cave (Fig. 4.2-1). De Souza et al. (2019) further examined the relationship between speleothem records and the duration of archaeological cultures in the *Llanos de Moxos* and southwestern Amazon (namely, the state of Acre, Brazil) (Fig. 4.2-1). Both were occupied by archaeological cultures with different duration and distribution. The former is characterized by two main archaeological cultures – monumental mounds or *lomas* and ring ditches or *zanjas*. The latter is defined by the presence of geometrical enclosures (geoglyphs) and circular mound villages (de Souza et al. 2019) (Fig. 4.5.4-1).

Geoglyph culture in the southwestern Amazon (400 BCE to 1000 CE) reached a construction apex between 400 BCE to 400 CE. This period, is synchronous with a relatively stable climate, documented throughout the Amazon basin (discussed in Session 4.5.3). This period exhibits major transformations throughout the Amazon, with the onset and spread of ceramic traditions, a more sedentary lifestyle and practices of polyculture agroforestry (forest farming), which has been linked to a more humid climate and forest expansion/stabilization in ecotonal Amazon regions such as Laguna Bella Vista and Chaplin (Neves, 2013; Iriarte et al. 2020; Souza et al. 2020). Further south, in the Llanos de Moxos region, monumental mounds were only built starting at 400 CE and thrived during the prolonged drier MCA climate (Fig. 4.5.4-1), which is coherent with their more extensive burning of the savannas and the construction of irrigation canals for drainage or cultivation (Souza et al., 2019). Over the eastern Amazon (Paraíso cave region), evidence of large, sedentary and complex pre-Columbian populations during this period is provided by the Marajoara culture. Just after 400 CE, Marajoara sites reach their peak, and the culture thrived during the MCA period (700–1100 CE) (Souza et al., 2019), when the Paraíso paleoclimatic record documents wetter conditions.

De Souza et al. (2019) and Riris (2019), argue that the connection between the Geoglyph demise in 1000 CE and the regional drought documented by paleoclimatic records in the southwestern Amazon should be interpreted with caution. Geoglyphs do not normally contain evidence of habitation, and are currently interpreted as a form of ceremonial architecture (Saunaluoma and Schaan, 2012). Therefore, their abandonment may be unrelated to any climate-driven demographic trend. We note that relative changes in monsoon strength documented by $\delta^{18}O$ values in speleothems may have been insufficient to significantly affect the economic basis of societies living in the southwestern Amazon. Societies elsewhere in the basin practicing similar forms of agroforestry, as documented in the Geoglyphs (Watling et al. 2017), were seemingly unaffected by the MCA drought (Souza et al., 2019).

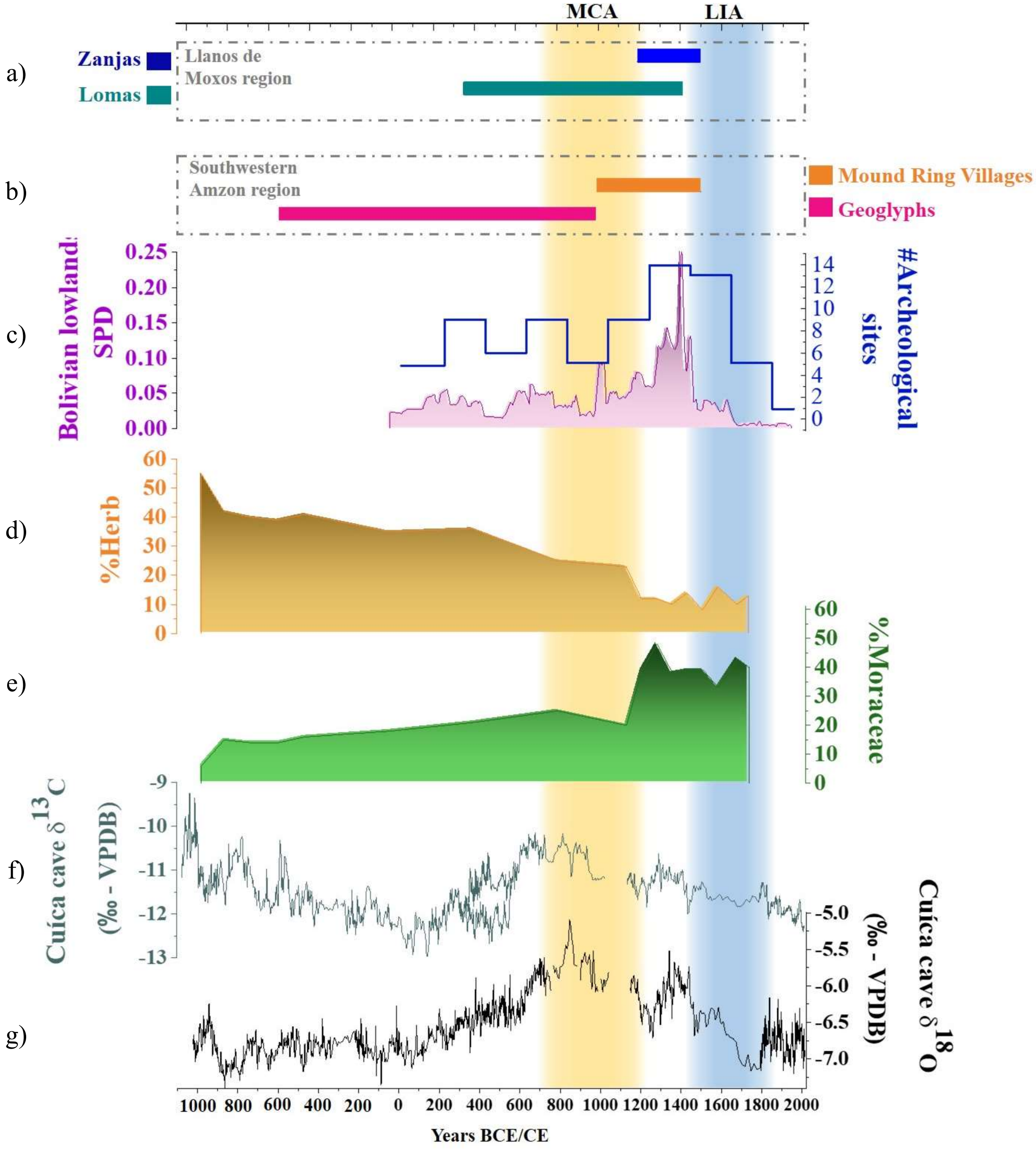

Figure 4.5.4-1 – a) Period of occurrence of archeological records from Llanos de Moxos region, comprising the Lomas (green) and Zanjas (blue) cultures (Souza et al., 2019); b) Same as a), but from Southwestern Amazon region, comprising the Geoglyphs (pink) and Mound Ring Villages (orange) cultures (Souza et al., 2019); c) SPD records from Bolivian lowlands region archeological sites and number of archeological sites within this region (Maezumi et al., 2018); d) Laguna Chaplin pollen records indicative of savanna swamps (%Herbs) (Maezumi et al., 2018); e) Laguna

Chaplin pollen records indicative of rainforest (%Moraceae) (Maezumi et al., 2018); f) Cuíca cave $\delta^{13}C$ record; g) Cuíca cave $\delta^{18}O$ record.

The Geoglyph demise during the MCA is followed by the emergence of the Mound Ring Villages. We suggest these populations may have taken advantage of a more open vegetation, considering the evidence for earthworks (causeways, roads) connecting the sites over long distances, and that it is unlikely that widespread clearance was practiced (Carson et al., 2014; Iriarte et al., 2020; Saunaluoma et al. 2021; Kukla et al., 2021). The transition period between MCA and LIA, when the paleoclimate records from the Amazon basin present very heterogonous conditions, was also marked by significant demographic changes documented by archaeological data (Fig. 4.5.4-1).

The period of 1300-1450 CE is characterized by elevated isotopic values in both $\delta^{18}O$ and $\delta^{13}C$ records from Cuíca cave, indicating a weak monsoon and a possible opening of vegetation, along with a slight increase of Herbs seen in the LCH record (Fig. 4.5.4-1). This period follows a peak in the archaeological occupation of the basin, with the spread of major ceramic traditions and landscape modification, including anthropogenic dark earths; however, it is also a period of apparent stabilization, with the radiocarbon record suggesting that Amazonian populations may have reached carrying capacity in the three centuries prior to the European arrival (Arroyo-Kalin and Riris, 2021). We further suggest that the overall decrease in SAMS intensity may have led to a more open and flammable vegetation, thus more accessible to human occupation, which also is a possible forcing on the environment and vegetation transformation. This is corroborated by Carson et al. (2014), who propose that pre-Columbian populations took advantage of a more open landscape for settlement rather than applying excessive efforts for clearing and burning a denser-canopy location.

The subsequent LIA period is characterized by a precipitation dipole over the Amazon basin. The wetter stage documented by the Cuíca $\delta^{18}O$ record and western Amazon records is clearly concurrent with the cultural transitions observed in the southwestern Amazon, i.e. from the monumental mounds to the ring ditches, and from the Geoglyphs to the mound villages, respectively (Souza et al., 2020) (Fig. 4.5.4-1). In contrast, however, eastern and central Amazonian populations seem to abide and even flourish during the drier scenario documented by Paraíso (Souza et al., 2019). The fact that this is also the period of the European conquest in South America, which is the primary driver for the demise of the majority of pre-Columbian cultures

(Koch et al. 2019 and others), confounds our assessment of how climate change may have affected demography during this period.

4.6 Supplementary Material

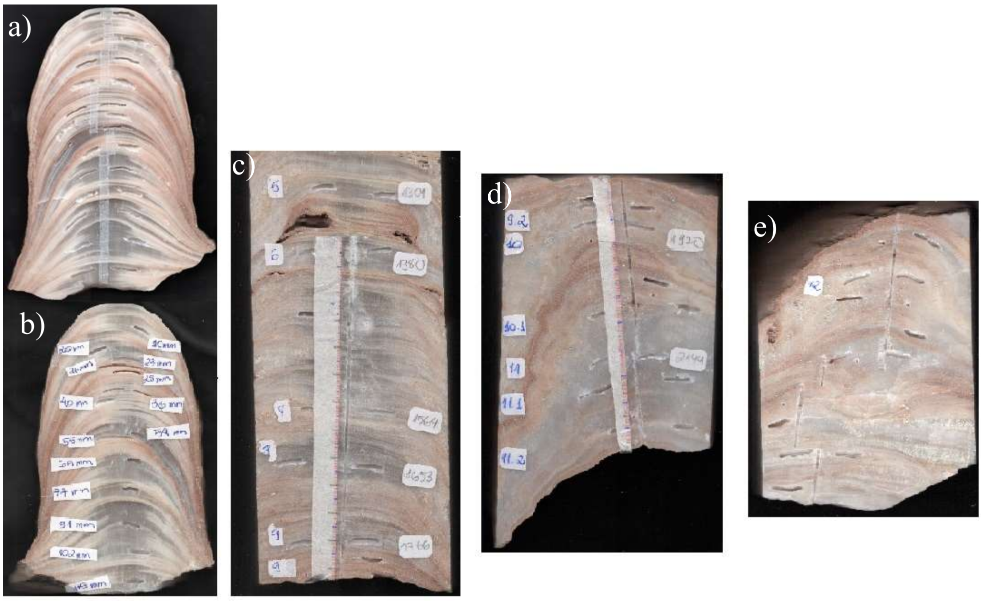

Figure 4.6-1- a) Face of stalagmite PIM4 where the $\delta^{18}O$ samplings were taken, in addition to sampling for U/Th; b) Face of stalagmite PIM4 where additional samplings for U/Th were obtained; c) First section of stalagmite PIM5, where ^{18}O and U/Th were made; d) same as c, but the second section of PIM5; e) same as c, but for the third section of PIM5.

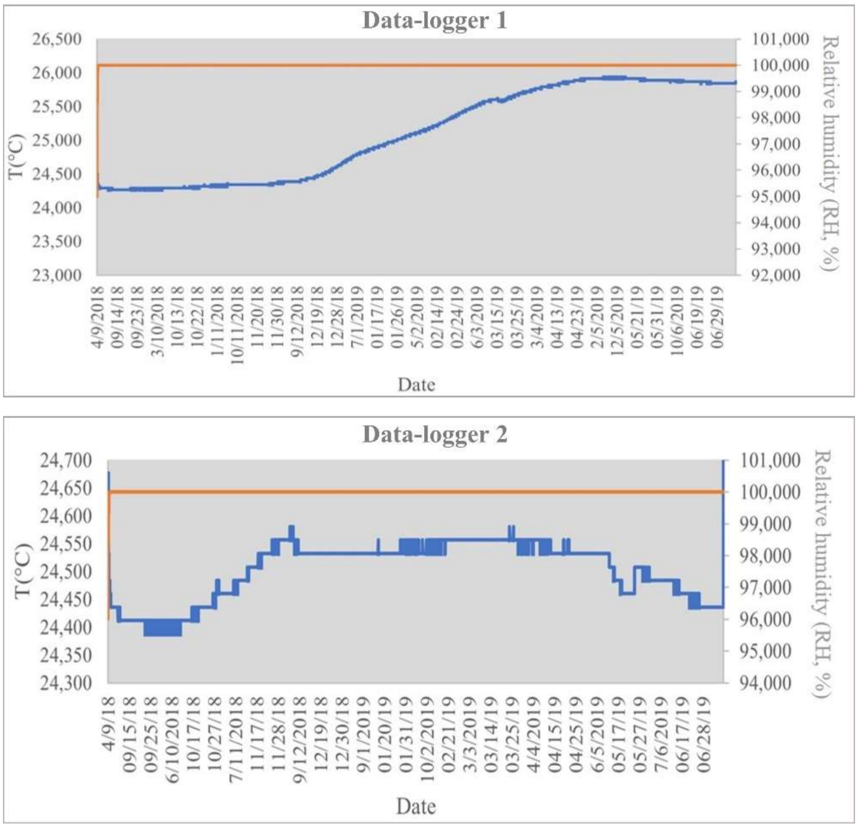

Figure 4.6-2 - Temperature (blue line) and relative humidity (orange line) records measured by data loggers 1 (TH1) and 2 (TH2) from 04/09/2018 to 08/07/2019 in the Cuíca cave hall where the speleothems were collected.

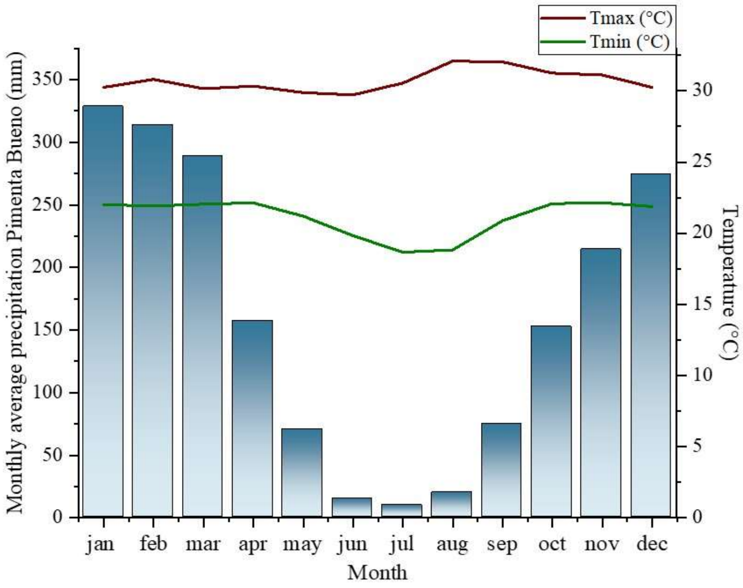

Figure 4.6-3 - Monthly average precipitation (blue bars), monthly average maximum (purple line) and minimum (green line) temperatures recorded at Pimenta Bueno ANA (AgênciaNacional de Águas) meteorological station from (1971-2016).

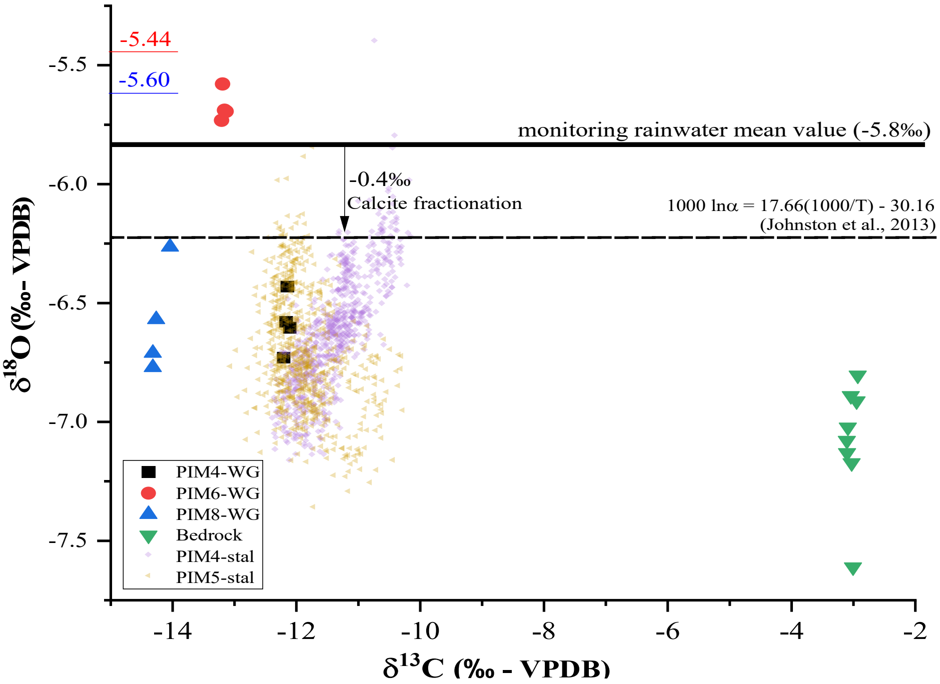

Figure 4.6-4 - Dispersion graph of obtained oxygen and carbon isotope values PIM4 (black square), PIM6 (red dot) and PIM8 (blue triangle) monitoring watch glasses (WG), from a sample of the bedrock (green triagle), and PIM4 (purple dots) and PIM5 (orange dots) speleothems. The small red and blue lines indicate the δ^{18}O value from drip water of PIM6 and PIM8 dripping sites, respectively. The black line is the δ^{18}O average of the 40 rainwater samples collected during one hydrological year near the cave site (~2km). The dashed line is the calculated calcite fractionation due to the cave average temperature of 25°C, based on Johnston et al. (2013).

5. RESULTS

5.1. Geochronology and Growth Rates

The total amount of 114 U/Th dates were produced for Cuíca cave speleothems, distributed over the stalagmites PIM2 (12), PIM3 (18), PIM4 (21), PIM5 (28), PIM6 (6), PIM7 (2), PIM8 (17), PIM-M-1 (6), PIM-M-2 (2), and PIM-M-3 (2). The goal with these samples and U/Th dates was either to have coeval speleothem records that goes back the last 3000 BP (1000 BCE) and to precisely constrain the higher resolution isotopic data in time in order to allow the discussion of high frequency climate variability in Amazon region. Attending these goals, the samples PIM4 and PIM5 were chosen for this study amongst the set speleothems dated during this study (Fig. 5.1-1).

PIM4 presents an almost continuous record from 338-2013 CE, with a 108-year hiatus from 1040-1148 CE (Fig. 5.1-2). The 2σ-errors of PIM4 U/Th ages present an average of 8 years, with errors ranging from 3-13, and only one 2σ-error of 44. The 2σ-errors yield typically < 1% error, but PIM4 yields ≤ 2% errors in most samples, likely because of very low ^{230}Th content in young samples that grew within last two centuries in modern time, rising the % the age uncertainty. For instance, a 3 year 2σ-error in 1997 CE yields in 13% of error, whereas a 3 year 2σ-error in 1146 CE yields in 0.34% of error. PIM5 presents a continuous record between 930 BCE - 570 CE (Fig. 5.1-2). Its 2σ- U/Th uncertainties present an average of 13 years, with 2σ-errors ranging from 5-35, and the 2σ-errors are typically ≤1% with an average value of 0.6% error.

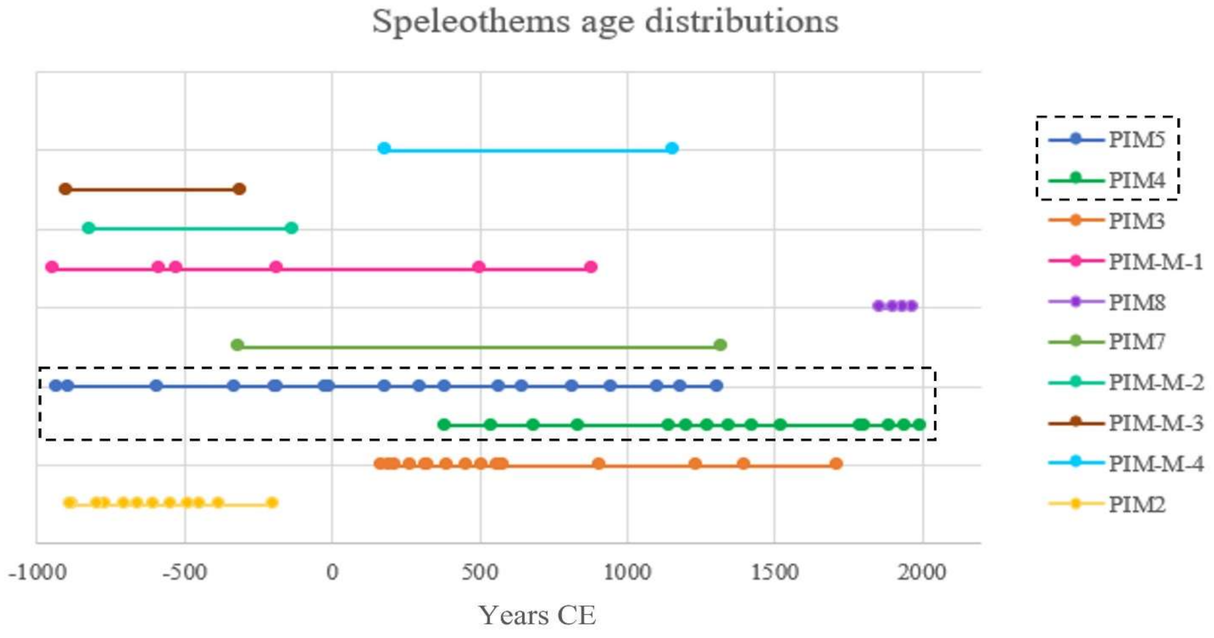

Figure 5.1-1 – U/Th date distribution along speleothems from Cuíca cave. The samples PIM4 and PIM5 (highlighted by the dashed rectangle) were investigated in this research because they together cover the entire time interval covered by all dated speleothems.

PIM4 growth presents five main stages, where the first is between 362-689 CE and presents a range of growth-rate (GR) between 0.19-0.13 mm/year (Fig. 5.1-3). After that, the GR drops to 0.02 mm/year in 739 CE and reaches 0.005 mm/year in 1046 CE, rising again from 1148 to 0.09 mm/year. The GR remains low between 0.09-0.05 mm/year until 1424 CE, when the values drop again to 0.03-0.01 mm/year until 1794 CE, when it recovers to higher GR (0.2-0.1 mm/year) until present day.

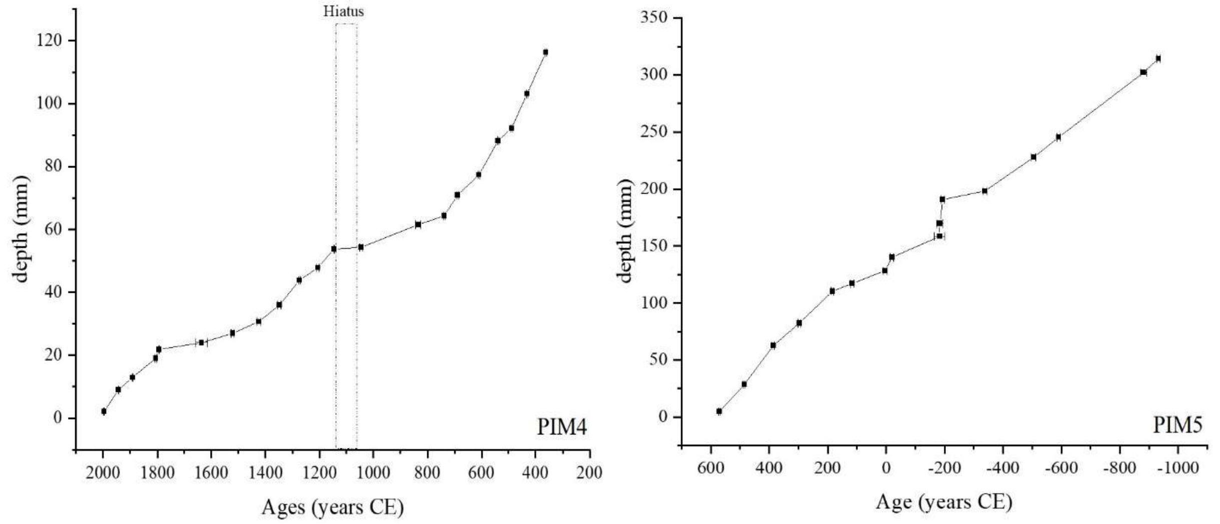

Figure 5.1-2 – U/Th date distribution from top to bottom of PIM4 (left) and PIM5 (right) speleothems. Horizontal bars represent the 2σ errors of the U/Th ages.

PIM5 has an average GR values of 0.34 mm/year (Fig. 5.1-3), which is significantly higher than the observed in the other Cuica speleothems. In the period between 193 and 184 BCE, the growth rate increases to 2.1 mm/year in average. In general, the GR values range from 0.49-0.05 mm/year. It's noteworthy that GR first presents a rather stable growth from -931 to -337 CE, when it drops to the lowest GR values (0.05 mm/year) and progressively increases until 570 CE with a GR of 0.28 mm/year.

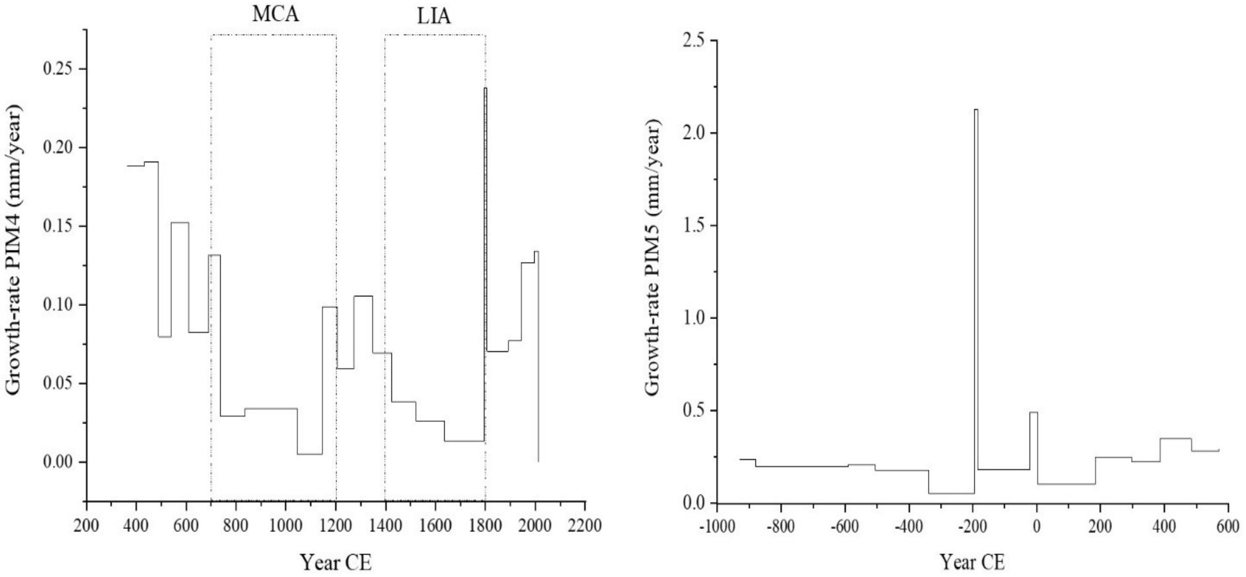

Figure 5.1-3 - Growth rates from PIM4 (left) and PIM5 (right). The dashed bars represent the period of Little Ice Age (LIA) a Medieval Climate Anomaly (MCA).

5.2. Statistical Analysis

The REDFIT spectral analysis (Schulz and Mudelsee, 2002) of the composite δ^{18}O record is predominantly marked by multidecadal, decadal and sub-decadal variabilities, revealing periodicities at 30 years above 95% significance and 17, 12, 9 and 7 years above 99% significance (Fig. 5.2-1), which can also be observed in the wavelet transform analysis (Fig. 5.2-2). However, considering two stalagmites are being investigated, it was also performed wavelet and REDFIT analysis of the δ^{18}O record from PIM4 and PIM5 separately.

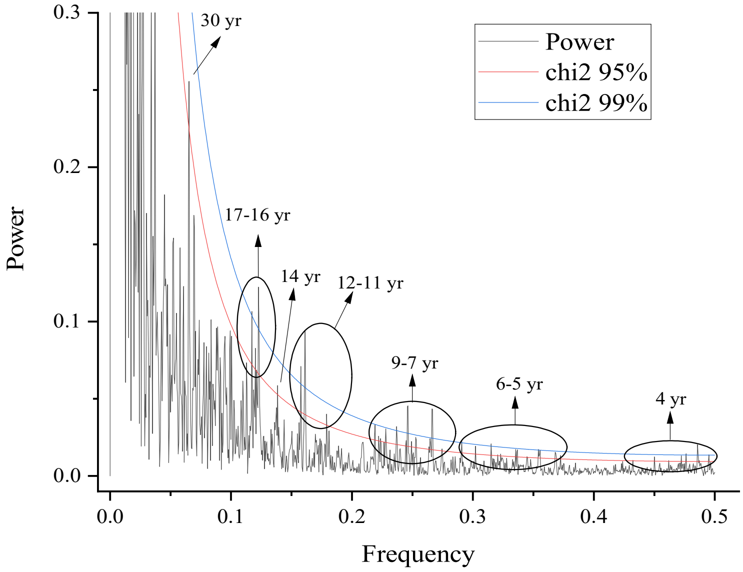

Figure 5.2-1 - REDFIT spectral analysis of Cuíca composite $\delta^{18}O$ record evenly-spaced in 2 years, where the numbers pointed by the arrows represent the most significant record frequencies, where red (blue) numbers represent 95% (99%) statistical significance.

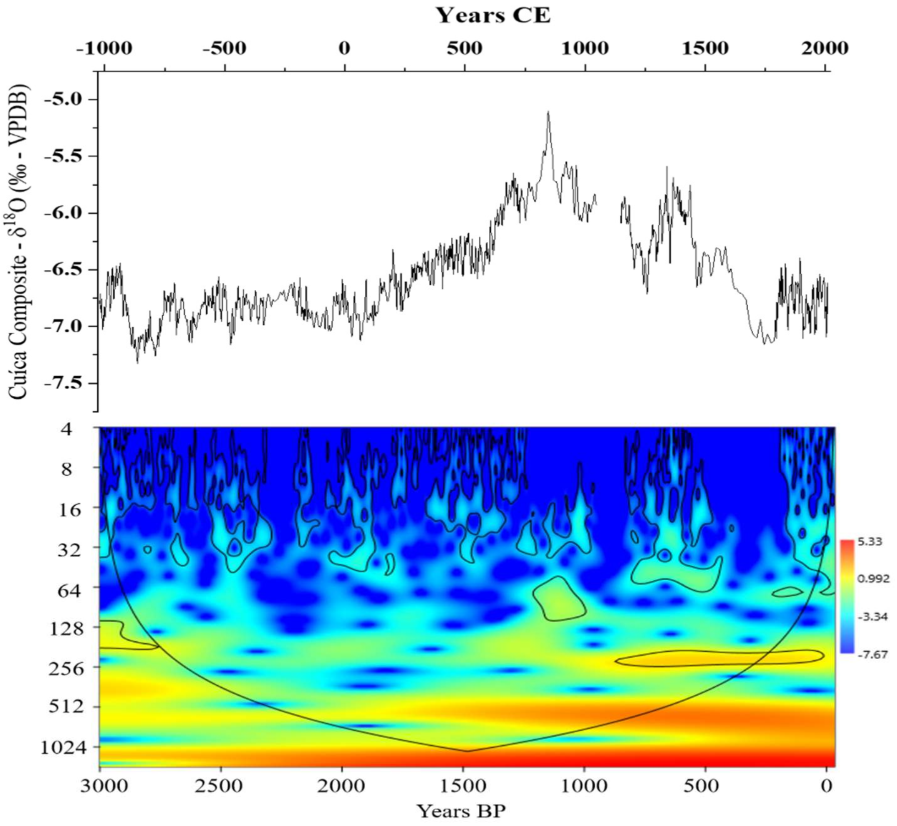

Figure 5.2-2 – (top) Cuíca composite $\delta^{18}O$ record and (bottom) wavelet analysis of PIM5 record evenly-spaced in 2 years, where the y axis represents the periodicities values, the x axis the time interval from the analyzed record, and the color index related to the intensity of the event, being red (blue) for more (less) intense. The outline in black indicates the events that have statistical significance higher than p=0.05. The conic section indicates the data reliance for the areas inside the cone.

The same periodicities ranging approximately from 30 to 4 years observed in the composite wavelet and REDFIT analysis are also evident in both stalagmites in their REDFIT and wavelet analysis (Fig. 5.2-3 and 5.2-4). Further multidecadal periodicities between ~30-60 years and ~64-128 years are also evident at 95% significance in both PIM4/5 $\delta^{18}O$ record wavelet analysis (Fig. 5.2-4). However, both these ranges only appear in PIM5 record around 2000 BP (0 CE), whereas for PIM4 these periodicities are present throughout the entire wavelet analysis, then indicating that they are more evident in the last 2000 years in the cuica record.

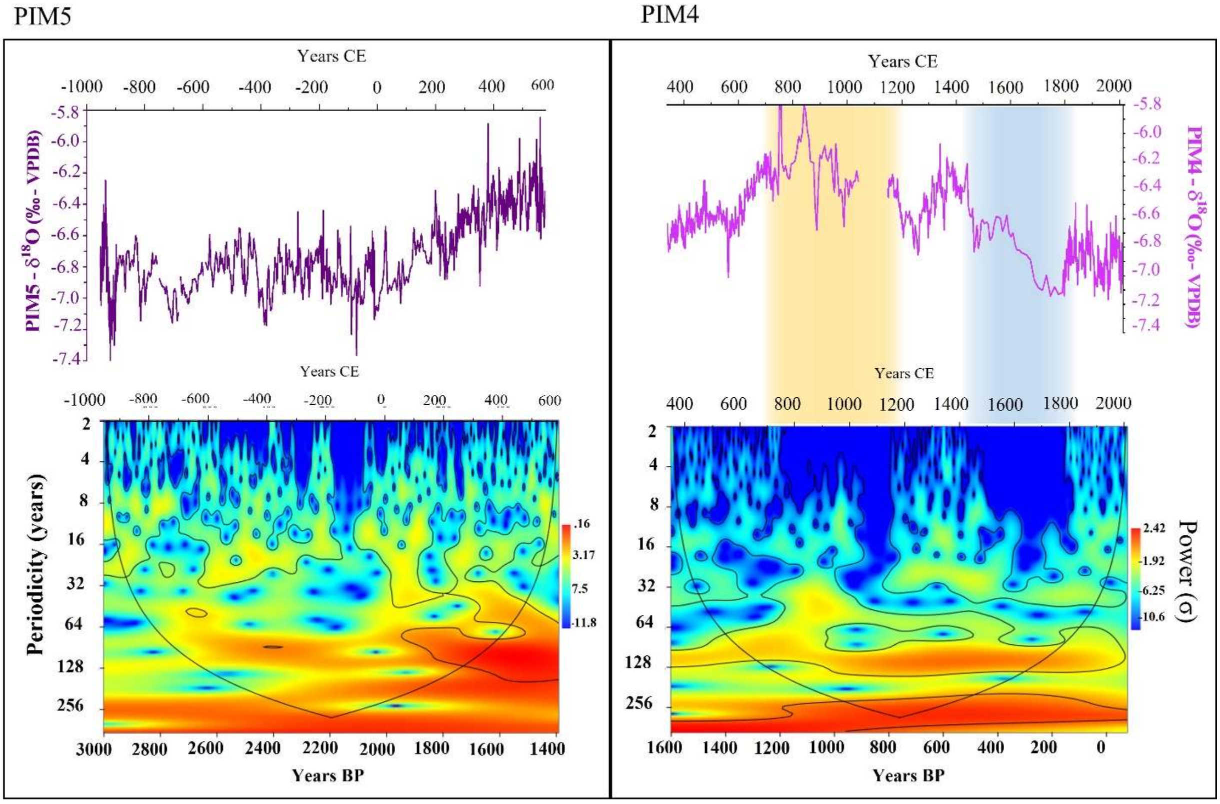

Figure 5.2-3 – (top left) PIM5 $\delta^{18}O$ record (dark purple) and wavelet analysis of PIM5 record evenly-spaced in 2 years (bottom left), where the y axis represents the periodicities values, the x axis the time interval from the analyzed record, and the color index related to the intensity of the event, being red (blue) for more (less) intense. The outline in black indicates the events that have statistical significance higher than p=0.05. The conic section indicates the data reliance for the areas inside the cone. (top right) Same as "top left", but for PIM4 $\delta^{18}O$ record (light purple). (bottom right) Same as "bottom left", but for PIM4 $\delta^{18}O$ record. The rectangle in orange (blue) indicates the MCA (LIA) period.

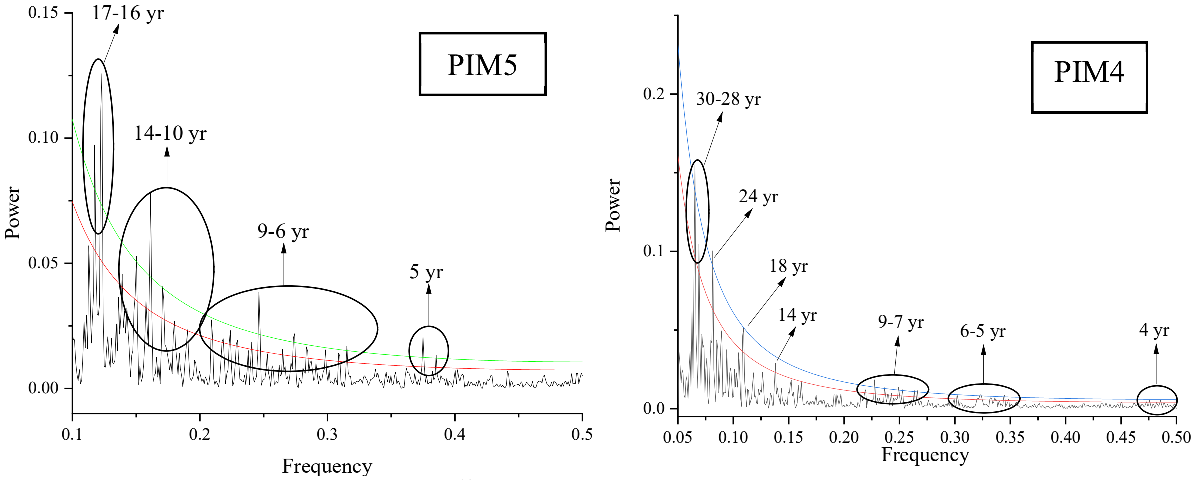

Figure 5.2-4 - REDFIT spectral analysis $\delta^{18}O$ records evenly-spaced in 2 years of PIM5 (left) and PIM4 (right). Arrows represent the most significant record frequencies, where red line represent 95% statistic reliability and blue or green lines represent 99%.

6. DISCUSSION

Decadal to multi-decadal variability observed on the $\delta^{18}O$ record from Cuíca cave highlight that SAMS has been constantly subjected to climatic fluctuations at these time scales over the past three millennia. These variability in the SAMS were investigated in several studies that related it to sea surface temperatures (SSTs) fluctuations in tropical Atlantic ocean (e.g. Apaéstegui et al., 2014; Novello et al., 2012), in the Pacific ocean (e.g. Grimm and Tedeschi, 2008), and solar irradiance (e.g. Novello et al., 2016).

Previous studies have pointed out the effect of distinct AMO phases in precipitation variability over SAMS regions (e.g. Apaéstegui et al., 2014; Chiessi et al., 2009; Knight et al., 2006; Jones & Carvalho, 2018). Indeed, a comparison between Cuíca $\delta^{18}O$ record with AMO reconstruction (Mann et al., 2009) shows that the trend toward a negative AMO phase and the establishment of this phase is concurrent with a wetter scenario over the monsoon region during the LIA, such as suggested by the studies mentioned above (Fig. 6-1). In addition, the typical ~64-80 year periodicity found for AMO cycles is evident throughout most of PIM4 wavelet analysis, indicating a persistent mode of variability within this range of time.

Therefore, it is possible to state that AMO has played an important role in SAMS variability over most of the last two millennia based on these evidences. However, to understand the effect of AMO on SAMS in more detail is still challenging. First because the ~64-80 years periodicity is mainly observed in PIM4 stalagmite and is only statistically significant in the younger portion of the PIM5 wavelet analysis until ~100 CE when the $\delta^{18}O$ record starts to shift towards a climate anomaly (Fig. 5.2-3). Second because the studies making this association indeed correlate the AMO phases with changes in SAMS based on statistics and climate models (Jones & Carvalho, 2018) or additional direct association between records (e.g. Apaestegui et al., 2014; Chiessi et al., 2009; Novello et al., 2012), however none of them address more central regions of SAMS domain, such as southwestern Amazon Basin.

Nonetheless, a recent study by Mann et al. (2021) brought up new evidence that AMO-like variations observed in paleoclimatic proxies are more likely a result of explosive volcanic activity and natural changes in solar radiative forcing rather than an internal Atlantic Ocean variation mode. In a comparison between the reconstruction of a global volcanic forcing (GVF - Sigl et al., 2015) and South American temperature proxy records, Lüning et al. (2019) state that the low-high-low volcanic activities form early-MCA (950-1100 CE), late-MCA (1100-1350 CE) and mid-LIA

(1350-1600 CE), respectively, do not correspond to the climatic signal observed for the temperature records. However, the comparison with temperature might not be applicable for precipitation changes. For instance, two periods of high volcanic activities (1100-1350 CE and 1600-1850 CE) agree with a wet excursion in late-MCA and the wetter conditions in LIA, respectively, evidenced by Cuíca record. This could be an initial indication of a volcanic forcing role on precipitation changes over South America, yet further investigation is needed.

Also, Lüning et al. (2019) suggest a relevant solar forcing component to the events of MCA and LIA, which are characterized generally by high and low solar activity, respectively, thus driving to the drier MCA and wetter LIA scenarios observed in regions affected by SAMS. Even though the physical processes that might relate solar activity and ocean cycles to climate have still a lot to be understood, the combination of high (low) solar activity with a positive (negative) ocean cycles suggest a significant impact of these forcings over South American climate (Lüning et al., 2019).

As for NAO, decadal periodicities characteristically of this ocean mode (Trouet et al., 2009) are consistent throughout most of PIM4 and PIM5 wavelet analysis with high significance (>95%) and are also significant in the respective REDFIT analysis, yet not much has been discussed about its role over South America and SAMS in past climate times. Apaestegui et al. (2014) bring up a possible link between NAO with distinct rainfall patterns over eastern Andes (Palestina cave record) and Northeastern Brazil (Diva de Maura cave record, Novello et al., 2012), again on western/easternmost regions of tropical South America, respectively. Yet, they state that the variations observed might be a result of Pacific-Atlantic Ocean interactions, since clearly distinguishing the superimposed variations of ocean cycles is difficult, thus similarly challenging to link direct variations of NAO with general SAMS activity.

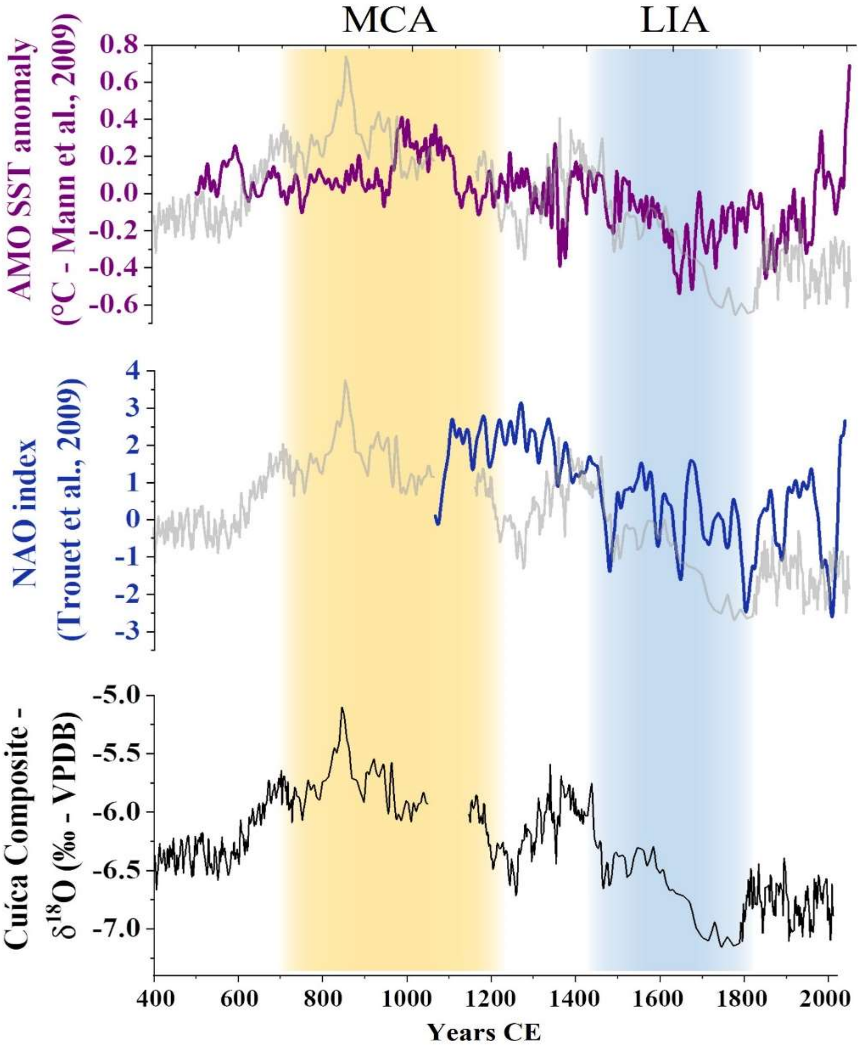

Figure 6-1 – (top) AMO related SST anomalies (Mann et al. 2009) in purple; (middle) NAO Index (Trouet et al., 2009) in blue; (bottom) Cuíca cave $\delta^{18}O$ record in black. The Cuíca cave $\delta^{18}O$ record is also in light gray behind both AMO and NAO reconstructions. The orange (blue) rectangle is representative of MCA (LIA) period.

Given the tropical Atlantic Ocean is the greatest source of moisture for southwestern Amazonia and SAMS core region, both NAO and AMO-like variations likely played a significant role during LIA climate anomaly. Several ocean/atmospheric cycles, including NAO and the AMO-like variation, were in a negative phase, meaning a cooling of North Atlantic, which has been previously related to an increase in South American precipitation (e.g. Chiessi et al., 2009; Knight et al., 2006; Jones & Carvalho, 2018). In addition to Cuíca $\delta^{18}O$ record at SAMS core region, other western Amazonia/southwestern Brazil records under SAMS/SACZ also report wetter conditions during LIA, what corroborates to a heightened moisture influx into the continent leading to an enhanced SAMS/SACZ activity (see discussion 4.5.3).

In addition to the effects of the Atlantic ocean climate conditions on South America, impacts of multidecadal modes from the Pacific ocean on the continent, such as the IPO and PDO, have also been discussed (see section 2.5). Regarding IPO variations (Buckley et al., 2019), it remained majorly in positive phases throughout the record's length, which spans from pre-LIA to the present. During LIA period Cuíca cave $\delta^{18}O$ record is characterized by a significant wetter stage, which might indicate an IPO influence on positive precipitations anomalies over southwestern Amazon according to the climate models observed in Buckley et al. (2019). Moreover, both wavelet and REDFIT analysis from PIM4 show persistent periodicities ranging between 30-20 years during the interest period, which are consistent with both IPO and PDO phase changes (Biondi et al., 2001; MacDonald & Case, 2005; Kayano &Andreoli, 2007; Dong & Dai, 2015; Buckley et al., 2019), and therefore might indicate the influence of these modes on multidecadal precipitation variabilities over southwestern Amazon.

Even though IPO trend agree with Cuíca $\delta^{18}O$ record during LIA and with previous climate models, a careful approach is needed when making these comparisons given that, yet, limited climatology studies have been done regarding IPO's influence over South America, and more specifically over southern/southwestern Amazon basin, therefore further investigation is necessary. As for PDO, its direct effects over climate at the present region of study are more complex to elaborate since most studies on that subject discuss the effects of PDO-ENSO jointly variations over South America (e.g. Kayano & Andreoli, 2007; Silva et al., 2011), since they share strong teleconnections. In general, when PDO and ENSO are both in their warm (positive) phase, a stronger effect on precipitation is observed in South America, leading to a drought over eastern Amazon and likely to a wetter period over western/southwestern Amazon (Silva et al., 2011).

Finally, interannual variations in South America climate have been related to ENSO modes, which was proven to play an important role on climatic patterns in several regions in the continent and regions within SAMS influence (e.g. Garreaud et al., 2009; Grimm & Tedeschi, 2008). However, correlations between ENSO episodes and precipitation over South America in Garreaud et al. (2009) reveal that our site in southwestern Amazonia is not a region under great influence of ENSO episodes as much as other areas (southeastern/western, western, and northeastern South America) that suffer extreme climate events due to El-Niño activity. Still, our record does documents periodicities of 7-4 years with high significance (ENSO episodes timescales of 2-7 years – Hanley et al., 2003), what indicates that ENSO may affect the site on interannual timescales, yet in a milder way when compared with these other regions.

Effects of El-Niño episodes are well-known for typical climatic patterns on regions highly affected by it, such as opposite precipitation modes between Peruvian Andes and southeast Brazil. Thereby, the fact that our site is not highly affected by El-Niño episodes (especially in longer timescales) along with $\delta^{18}O$ records from Cuíca, Peruvian Andes and southeastern Brazil trending to a wet LIA precludes the role of ENSO as a main factor causing one of the major changes in SAMS and this continental-scale precipitation dipole (Vuille et al., 2012). The long-term changes of heighten monsoon activity are then associated with enhanced moisture influx from tropical Atlantic leading to an increase in convective activity over the core SAMS domain (Vuille et al., 2012; Campos et al., 2019; Novello et al. 2018).

7. CONCLUSIONS

The paleoclimatic reconstruction for the last three thousand years based on stable isotopes from speleothems collected in Cuíca cave in southwestern Amazon Basin contributes in an unprecedented way the understanding of the SAMS and its influence on climate dynamics over the continent. It allowed to assess SAMS behavior and continental moisture distribution during important worldwide climate changes, such as MCA and LIA, what is a great asset for further contributions with climate modeling research and with future climate prediction.

The evidence gathered here from the new $\delta^{18}O$ record from Cuíca cave speleothems, along with isotope-enabled model analysis, indicates that the variations in $\delta^{18}O$ within the last 3000 years are indeed a reflection of monsoon variability. Here we investigate the climatic variations throughout the Amazon basin over the last 3k years characterized by four distinct periods: 1) 1020 BCE to 300 CE, when records throughout the basin point to a more uniform climatic pattern indicating neutral SAMS conditions; 2) 950-1250 CE (MCA period), with drier conditions established over the majority of the Amazon basin; 3) 1260-1450 CE, the transition period between the MCA and LIA characterized by heterogenous climate conditions over the Amazon basin; 4) 1450 to the present, marked by the establishment of an E-W precipitation dipole over the Amazon basin and, in a more expanded view, tropical South America, when the western-southwestern Amazon/SAMS and central-western Brazil/SACZ regions are wetter compared to the drier eastern/northeastern regions.

The $\delta^{13}C$ record from Cuíca cave documents an expansion of vegetation between 1020 BCE and 200 CE, followed by a retraction and expansion during the MCA and LIA periods, respectively. These findings are in agreement with vegetation reconstructions of the Amazon basin indicating Moraceae and Herbs taxas from the laguna Chaplin near the Cuíca site. The interplay between past climate and environmental changes with pre-Columbian cultures is complex which makes it difficult to establish cause-and-effect relationships.

The statistical analysis performed for the speleothems data reveal significant interannual, decadal, and multidecadal periodicities that are, in general, mostly associated with SSTs anomalies in the Atlantic Ocean and atmospheric circulations. ENSO influence over the study site does not seem to be one of the most important forcings for relevant changes in precipitation patterns, yet interannual periodicities are likely related to its changes between positive/negative phases and they are present throughout the entire studied period. IPO variations might play a role on southwestern

Amazon climate, where positive phases would lead to positive precipitation anomalies, yet further investigation is needed.

Variations as the AMO-like in Atlantic SSTs are likely associated with the multidecadal periodicities observed in Cuíca record, but they seem to be more relevant after the onset of climatic anomalies in Cuíca oxygen isotope record at ~100 CE, indicating that these variations might have played an important role on anomalous SAMS variations. On the other hand, decadal oscillations are likely associated with NAO atmospheric circulation and are present throughout the entire record, as evidenced by both wavelet and REDFIT analysis of PIM4/5 speleothems, pointing out a continuous influence of this system on variations in precipitation over the study area. The comparison For the MCA period, however, the AMO reconstruction does not present substantial changes that could corroborate its influence on the changes observed for the study site. In addition, the lack of data for NAO reconstruction further into the MCA period hampers a more complete understanding on the influence of this system during this anomaly at the site. In summary, it is more difficult to establish a role of these systems for the climatic changes observed in Cuíca record during MCA.

8. REFERENCES

Alexander, M. A., Halimeda Kilbourne, K., & Nye, J. A. , 2014, Climate variability during warm and cold phases of the Atlantic Multidecadal Oscillation (AMO) 1871–2008: Journal of Marine Systems, v. 133, p. 14-26, doi:10.1016/j.jmarsys.2013.07.017.

Ampuero, A., S. et al., 2020, The Forest Effects on the Isotopic Composition of Rainfall in the Northwestern Amazon Basin: Journal of Geophysical Research: Atmospheres, v. 125, p. 1-16, doi:10.1029/2019JD031445.

Apaéstegui, J. et al., 2014, Hydroclimate variability of the South American Monsoon System during the last 1600 yr inferred from speleothem isotope records of the north-eastern Andes foothills in Peru: Climate of the Past Discussions, v. 10, p. 533-561, doi:10.5194/cpd-10-533-2014.

Apaéstegui, J. et al., 2018, Precipitation changes over the eastern Bolivian Andes inferred from speleothem ($\delta^{18}O$) records for the last 1400 years: Earth and Planetary Science Letters, v. 494, p. 124-134, doi:10.1016/j.epsl.2018.04.048.

Arroyo-Kalin, M., & Riris, P., 2021, Did pre-Columbian populations of the Amazonian biome reach carrying capacity during the Late Holocene?: Philosophical Transactions of the Royal Society B: Biological Sciences, v. 376, p. 20190715, doi:10.1098/rstb.2019.0715.

Azevedo, V. et al., 2019, Medieval Climate Variability in the eastern Amazon-Cerrado regions and its archeological implications: Scientific Reports, v. 9, p. 1-10, doi:10.1038/s41598-019-56852-7.

Baker, A., Berthelin, R., Cuthbert, M. O., Treble, P. C., Hartmann, A., & Team, T. K., 2020, Rainfall recharge thresholds in a subtropical climate determined using aregional cave drip water monitoring network: Journal of Hydrology, v. 587, p. 125001. doi:10.1016/j.jhydrol.2020.125001.

Biondi, F., Gershunov, A., & Cayan, D. R. , 2001, North Pacific Decadal Climate Variability since 1661: American Meteorological Society, v. 14, p. 5-10, doi:10.1175/1520-0442(2001)014<0005:NPDCVS>2.0.CO;2.

Bird, B. W., Abbott, M. B., Vuille, M., Rodbell, D. T., Stansella, N. D., & Rosenmeier, M. F., 2011, A 2,300-year-long annually resolved record of the South American summer monsoon from the Peruvian Andes: Proceedings of the National Academy of Sciences of the United States of America (PNAS), v. 108, no. 21, p. 8583-8588, doi:10.1073/pnas.1003719108.

Buckley, B. M., Ummenhofer, C. C., D'arrigo, R. D., Hansen, K. G., Truong, L. H., Le, C. N., & Stahle, D. K. (2019). Interdecadal Pacific Oscillation reconstructed from trans-Pacific tree rings: 1350–2004 CE. Climate Dynamics, 53, pp. 3181-3196. doi:10.1007/s00382-019-04694-4

Cai, W. et al., 2020, Climate impacts of the El Niño– Southern Oscillation on South America: Nature Reviews Earth & Environment, v. 1, p. 215-231, doi:10.1038/s43017-020-0040-3.

Campos, J. L., Cruz, F. W., Ambrizzi, T., Deininger, M., Vuille, M., Novello, V. F., & Strikis, N. M., 2019, Coherent South American Monsoon Variability During the Last Millennium Revealed Through High-Resolution Proxy Records: Geophysical Research Letters, v. 46, no. 14, p. 8261-8270, doi:10.1029/2019GL082513.

Carlson, P. E. et al., 2020, Constraining speleothem oxygen isotope disequilibrium drivenby rapid CO_2 degassing and calcite precipitation: Insightsfrom monitoring and modeling: Geochimica et Cosmochimica Acta, v. 284, p. 222-238, doi:10.1016/j.gca.2020.06.012.

Carson, J. F., Whitney, B. S., Mayle, F. E., Iriarte, J., Prümers, H., Soto, J. D., & Watling, J., 2014, Environmental impact of geometric earthworkconstruction in pre-Columbian Amazonia: Proceedings of the National Academy of Sciences, v. 111, no. 29, p. 10497-10502, doi:10.1073/PNAS.1321770111.

Carson, J. F., Whitney, B. S., Mayle, F. E., Iriarte, J., Prümers, H., Soto, J. D., & Watling, J., 2014, Environmental impact of geometric earthworkconstruction in pre-Columbian Amazonia: Proceedings of the National Academy of Sciences, v. 111, no. 29, p. 10497–10502, doi:10.1073/pnas.1321770111.

Carvalho, L. M., & Dias, M. A., 2021, Mesoscale and High-Impact Weather in the South American Monsoon, *in* Chang, C.-P., Ha, K.-J., Johnson, R. H., Kim, D., Lau, G. N. C., Wang, B., ed., The Multiscale Global Monsoon System (fourth edition): Singapore, World Scientific, p. 151-160.

Carvalho, L. M., Jones, C., & Liebmann, B., 2002, Extreme Precipitation Events in Southeastern South America and Large-Scale Convective Patterns in the South Atlantic Convergence Zone: Journal of Climate, v. 15, p. 2377-2394, doi: 10.1175/1520-0442(2002)015<2377:EPEISS>2.0.CO;2.

Carvalho, L. M., Jones, C., & Liebmann, B., 2004, The South Atlantic convergence zone: Intensity, form, persistence, and relationships with intraseasonal to interannual activity and extreme rainfall: Journal of Climate, v. 17, p. 88-108, doi:10.1175/1520-0442(2004)017<0088:TSACZI>2.0.CO;2.

Cheng, H. et al., 2013a, Improvements in 230Th dating, 230Th and 234U half-life values, and U-Th isotopic measurements by multi-collector inductively coupled plasma mass spectrometry: Earth and Planetary Science Letters, v. 371-372, p. 82-90, doi:10.1016/j.epsl.2013.04.006.

Cheng, H. et al., 2013, Climate change patterns in Amazonia and biodiversity: Nature Communications, v. 4, p. 1-6, doi:10.1038/ncomms2415.

Chiessi, C. M., Mulitza, S., Pätzold, J., Wefer, G., & Marengo, J. A., 2009, Possible impact of the Atlantic Multidecadal Oscillation on the South American summer monsoon: Geophysical Research Letters, v. 36, p. L21707, doi:10.1029/2009GL039914.

Clark, I. D., & Fritz, P., 1997, Environmental Isotopes in Hydrogeology: Boca Raton, CRC Press,342p, doi:10.1201/9781482242911.

Cruz, F. W. et al., 2005, Stable isotope study of cave percolation waters in subtropical Brazil: Implications for paleoclimate inferences from speleothems: Chemical Geology, v. 220, p. 245–262, doi:10.1016/j.chemgeo.2005.04.001.

Cruz, F. et al., 2009, Orbitally driven east-west antiphasing of South American precipitation: Nature Geoscience, v. 2, no. 3, doi:10.1038/ngeo444.

Dong, B., & Dai, A., 2015, The influence of the Interdecadal Pacific Oscillation on Temperature and Precipitation over the Globe: Climate Dynamics, v. 45, p. 2667–2681, doi:10.1007/s00382-015-2500-x.

Dreybrodt, W., 2008, Evolution of the isotopic composition of carbon and oxygen in a calcite precipitating H_2O–CO_2–$CaCO_3$ solution and the related isotopic composition of calcite in stalagmites: Geochimica et Cosmochimica Acta, v. 72, no. 19, p. 4712-4724, doi:10.1016/j.gca.2008.07.022.

Edwards, R. L., Chen, J., & Wasserburg, G., 1986, 238U - 234U - 230Th - 232Th systemtics and the precise measurement of time over the past 500.000 years: Earth and Planetary Science Letters, v. 81, p. 175-192, doi:10.1016/0012-821X(87)90154-3.

Fairchild, I. J., & Baker, A., 2012, Speleothem Science: From Process to Past Environments: West Sussex, Wiley-Blackwell, 230p.

Fairchild, I. J. et al, 2006, Modification and preservation of environmental signals in speleothems: Earth-Science Reviews, v. 75, p. 105-153, doi:10.1016/j.earscirev.2005.08.003.

Fohlmeister, J., Voarintsoa, N., Lechleitner, F., Boyd, M., Brandstätter, S., Jacobson, M., & Oster, J. , 2020, Main controls on the stable carbon isotope composition of speleothems: Geochimica et Cosmochimica Acta, v. 279, p. 67-87, doi:10.1016/j.gca.2020.03.042.

Gamelin, B. L., Carvalho, L. M., & Kayano, M. , 2020, The combined influence of ENSO and PDO on the spring UTLS ozone variability in South America: Climate Dynamics, v. 55, p. 1539–1562, doi:10.1007/s00382-020-05340-0.

Gan, M. A., Kousky, V. E., & Ropelewski, C. F. , 2004, The South America Monsoon Circulation and Its Relationship to Rainfall over West-Central Brazil: American Meteorological Society, v.17, p. 47-66, doi:10.1175/1520-0442(2004)017<0047:TSAMCA>2.0.CO;2.

Garreaud, R. D., Vuille, M., Compagnucci, R., & Marengo, J. , 2009, Present-day South American climate: Palaeogeography, Palaeoclimatology, Palaeoecology, v. 281, no. 3-4, p. 180-195, doi:10.1016/j.palaeo.2007.10.032.

Ghil, M., Allen, M. R., Dettinger, M. D., Ide, K., Kondrashov, D., Mann, M. E., & Yiou, P. , 2002, Advanced Spectral Methods for Climatic Time Series: Reviews of Geophysics, v. 40, p. 3-1-3-41, doi:10.1029/2000RG000092.

Gray, S. T., Graumlich, L. J., Betancourt, J. L., & Pederson, G. T. , 2004, A tree-ring based reconstruction of the Atlantic Multidecadal Oscillation since 1567 A.D: Geophysical Research Letters, v. 31, no.12, p. L12205, doi:10.1029/2004GL019932.

Grimm, A. M., & Saboia, J. P. , 2015, Interdecadal Variability of the South American Precipitation in the Monsoon Season: Journal of Climate, v. 28, p. 755-775, doi:10.1175/JCLI-D-14-00046.1.

Grimm, A. M., & Tedeschi, R. G. , 2009, ENSO and Extreme Rainfall Events in South America ALICE: Journal of Climate, v. 22, p. 1589-1609, doi:10.1175/2008JCLI2429.1.

Haberle, S., & Maslin, M. , 1999, Late Quaternary Vegetation and Climate Change in the Amazon Basin Based on a 50,000 Year Pollen Record from the Amazon Fan, ODP Site 932: Quaternary Research, v. 51(1), p. 27-38. doi:10.1006/qres.1998.2020.

Hammer, Ø. , 2019, Manual Past 3.25.

Hanley, D. E., Bourassa, M. A., O'Brien, J. J., Smith, S. R., & Spade, E. R. , 2003, A Quantitative Evaluation of ENSO Indices: Journal of Climate, v. 16, no. 8, p. 1249–1258, doi:10.1175/1520-0442(2003)16<1249:AQEOEI>2.0.CO;2.

Hendy, C. H. , 1971, The isotopic geochemistry of speleothems. The calculation of the effects of different modes of formation on the isotopic composition of speleothems and their applicability as palaeoclimatic indicators: Geocochimica et Cosmochimica Acta, v. 35, p. 801-824, doi:10.1016/0016-7037(71)90127-X.

Hurrell, J. W., Kushnir, Y., Ottersen, G., & Visbeck, M. , 2003, An overview of the North Atlantic Oscillation: Geophysical Monograph, v. 134, p. 1-35, doi:10.1029/134GM01.

Iriarte, J. et al, 2020, The origins of Amazonian landscapes: Plant cultivation, domestication and the spread of food production in tropical South America. v. 248, p. 106582, doi:10.1016/j.quascirev.2020.106582.

Johnston, V. E., Borsato, A., Spötl, C., Frisia, S., & Miorandi, R. , 2013, Stable isotopes in caves over altitudinal gradients:fractionation behaviour and inferences for speleothem sensitivity to climate change: Climate of the Past, v. 9, p. 99–118, doi:10.5194/cp-9-99-2013.

Jones, C., & Carvalho, L. M. , 2018, The influence of the Atlantic multidecadal oscillation on the eastern Andes low-level jet and precipitation in South America: Climate and Atmospheric Science, v. 1, p. 1-7, doi:10.1038/s41612-018-0050-8.

Kanner, L. C., Burns, S. J., Cheng, H., Edwards, R. L., & Vuille, M. , 2013, High-resolution variability of the South American summer monsoon over the last seven millennia: Insights from a speleothem record from the central Peruvian Andes: Quaternary Science Reviews, v. 75, p. 1-10, doi:10.1016/j.quascirev.2013.05.008.

Karmann, I., Cruz, F. W., Viana, O., & Burns, S. J. , 2007, Climate influence on geochemistry parameters of waters from Santana–Pérolas cave system, Brazil: Chemical Geology, v. 244, p. 232–247, doi:10.1016/j.chemgeo.2007.06.029.

Kayano, M. T., & Andreoli, R. V. , 2004, Decadal variability of northern northeast Brazil rainfall and its relation to tropical sea surface temperature and global sea level pressure anomalies: Journal of Geophysical Research: Oceans, v. 109, p. C11011. doi:10.1029/2004JC002429.

Kayano, M. T., & Andreoli, R. V., 2007, Relations of South American summer rainfall interannual variations with the Pacific Decadal Oscillation: International Journal of Climatology, v. 27(4), p. 531-540, doi:10.1002/JOC.1417.

Kerr, R. A. , 2000, A North Atlantic climate pacemaker for the centuries: Science, v. 288(5473), p. 1984-1985, doi:10.1126/science.288.5473.1984.

Knight, J. R., Folland, C. K., & Scaife, A. A. , 2006, Climate impacts of the Atlantic Multidecadal Oscillation: Geophysical Research Letters, v. 33(17), p. L17706, doi:10.1029/2006GL026242.

Knudsen, M. F., Seidenkrantz, M.-S., Jacobsen, B. H., & Kuijpers, A. , 2011, Tracking the Atlantic Multidecadal Oscillation through the last 8,000 years: Nature Communications, v. 178, p. 1-8, doi:10.1038/ncomms1186.

Koch, A., Brierley, C., Maslin, M. M., & Lewis, S. L. , 2019, Earth system impacts of the European arrival and Great Dying in the Americas after 1492: Quaternary Science Reviews, v. 207(1), p. 13-36, doi:10.1016/j.quascirev.2018.12.004.

Kukla, T., Ahlströmb, A., Maezumi, S. Y., Chevaliere, M., Lu, Z., Winnick, M. J., & Chamberlain, C. P. , 2021, The resilience of Amazon tree cover to past and present drying: Global and Planetary Change, p. 202, doi:10.1016/j.gloplacha.2021.103520.

Lachniet, M. S. , 2009, Climatic and environmental controls on speleothem oxygen-isotope values: Quaternary Science Reviews, v. 28, p. 412-432.

Lauritzen, S.-E., & Lundberg, J. , 1999, Calibration of the speleothem delta function: an absolute temperature record for the Holocene in northern Norway: The Holocene, v. 9, p. 659-669.

Liebmann, B., Kiladis, G. N., Vera, C. S., Saulo, A. C., & Carvalho, L. M. , 2004, Subseasonal Variations of Rainfall in South America in the Vicinity of the Low-Level Jet East of the Andes and Comparison to Those in the South Atlantic Convergence Zone: Journal of Climate, v. 17(19), p. 3829-3842, doi:10.1175/1520-0442(2004)017<3829:SVORIS>2.0.CO;2.

Lu, Z., Liu, Z., Zhu, J., & Cobb, K. M. , 2018, A Review of Paleo El Niño-Southern Oscillation: Atmosphere, v. 9, no. 130, p. 1-27, doi:0.3390/atmos9040130.

Lüning, S., Gałka, M., Bamonte, F. P., Rodríguez, F. G., & Vahrenholt, F. , 2019, The Medieval Climate Anomaly in South America: Quaternary International, v. 508, p. 70-87, doi:10.1016/j.quaint.2018.10.041.

Macdonald, G. M., & Case, R. A. , 2005, Variations in the Pacific Decadal Oscillation over the past millennium: Geophysical Research Letters, v. 32, p. L08703, doi:10.1029/2005GL022478.

Maezumi, S. Y., Whitney, B. S., Mayle, F. E., Souza, J. G., & Iriarte, J. , 2018, Reassessing climate and pre-Columbian drivers of paleofire activity in the Bolivian Amazon: Quaternary International, v. 488, p. 81-94, doi:10.1016/j.quaint.2017.11.053.

Mann, M. E. et al, 2009, Global Signatures and Dynamical Origins of the Little Ice Age and Medieval Climate Anomaly: Science, v. 326, p. 1256-1260, doi:10.1126/science.1177303.

Mann, M., Steinman, B. A., Brouillette, D. J., & Miller, S. K. , 2021, Multidecadal climate oscillations during the past millenium driven by volcanic forcing: Climate Variability, v. 371, p. 1014-1019, doi:10.1126/science.abc5810.

Marengo, J. A. et al, 2012, Recent developments on the South American monsoon system: International Journal of Climatology, v. 32, p. 1–21, doi:10.1002/joc.2254.

Martineau, P., Nakamura, H., Kosaka, Y., & Yamamoto, A. , 2020, Importance of a vertically tilting structure for energizing the North Atlantic Oscillation: Scientific Reports, v.10, p. 12671, doi:10.1038/s41598-020-69551-5.

Mayle, F. E., & Power, M. J. , 2008, Impact of a drier Early–Mid-Holocene climate upon Amazonian forests: Philosophical Transactions of the Royal Society B, v. 363(1498), p. 1829–1838, doi:10.1098/rstb.2007.0019.

Miranda, I. S. , 2000, Floristic and structural analysis of wood vegetation of Comemoração River, Pimenta Bueno, Rondônia, Brazil: Acta Amazônica, v.30, no. 3, doi:10.1590/1809-43922000303422.

Neves, E. G. , 2013, Agriculture a Key Productive Activity in Pre-Colonial Amazonia. The Stable Productive Basis for Social Equality in the Central Amazon: Human-Environment Interactions: Current and Future Directions, p. 371-388, doi:10.1007/978-94-007-4780-7_16.

Novello, V. F. et al, 2012, Multidecadal climate variability in Brazil's Nordeste during the last 3000 years based on speleothem isotope records: Geophysical Research Letters, v. 39, no. 23, p. 1-6, doi:10.1029/2012GL053936.

Novello, V. F, 2019, Vegetation and environmental changes in tropical South America from the last glacial to the Holocene documented by multiple cave sediment proxies: Earth and Planetary Science Letters, v. 524, p. 115717, doi:10.1016/j.epsl.2019.115717.

Novello, V. F, 2018, Two Millennia of South Atlantic Convergence Zone Variability Reconstructed From Isotopic Proxies: Geophysical Research Letters, v.45(10), p. 5045-5051, doi:10.1029/2017GL076838.

Novello, V. F, 2017, A high-resolution history of the South American Monsoon from Last Glacial Maximum to the Holocene: Scientific Reports, v.8, p. 1-8, doi:10.1038/srep44267.

Novello, V. F, 2016, Centennial-scale solar forcing of the South American Monsoon System recorded in stalagmites: Scientific Reports, v.6, p. 1-8, doi:10.1038/srep24762.

Novello, V. F, 2021, Investigating $\delta^{13}C$ values in stalagmites from tropical South America for the last two millennia. Quaternary Science Reviews, v. 255, p. 1-10, doi:10.1016/j.quascirev.2021.106822.

Oliveira, C. E. , 2015, Rochas carbonáticas do estado de Rondônia: Informe de Recursos Minerais - Programa Geologia do Brasil, v.16, Porto Velho, Estado de Rondônia: CPMR.

Otto-Bliesner et al, 2016, Climate Variability and Change since 850 CE: An Ensemble Approach with the Community Earth System Model: Bulletin of the American Meteorological Society, v. 97(5), p. 735–754, doi:10.1175/BAMS-D-14-00233.1.

Pessenda, L. C., Gouveia, S. E., Ribeiro, A. d., De Oliveira, P. E., & Aravena, R. , 2010, Late Pleistocene and Holocene vegetation changes in northeastern Brazil determined from carbon isotopes and charcoal records in soils: Palaeogeography, Palaeoclimatology, Palaeoecology, v. 297, no. 3-4, p. 597-608, doi:10.1016/j.palaeo.2010.09.008.

Raia, A., & de Albuquerque Cavalcanti, I. F. , 2008, The life cycle of the South American monsoon system: Journal of Climate, v. 21, no. 23, p. 6227-6246, doi:10.1175/2008JCLI2249.1.

Rao, V. B., & Brito, J. I. , 1985, Teleconnections between the rainfall over northeast Brazil and the winter circulation of Northen hemisphere: PAGEOPH, v.123, p. 951–959, doi:10.1007/BF00876982.

Richards, D. A., & Dorale, J. A. , 2003, Uranium-series chronology and environmental applications of speleothems: Reviews in Mineralogy and Geochemistry, v. 52, p. 407–460, doi:10.2113/0520407.

Riris, P. , 2019, Sparse Radiocarbon Data Confound Culture-Climate Links in Late Pre-Columbian Amazonia: Quaternary, 2, p. 33, doi:10.3390/quat2040033.

Rizzotto, G. J., & Quadro, M. L. , 2007, Mapa Geológico do Estado de Rondônia: CPRM - Serviço Geológico do Brasil, Porto Velho. Retrieved from http://www.cprm.gov.br/publique/media/geologia_basica/cartografia_regional/mapa_rondonia.pdf

Salati, E., Dall'Olio, A., Matsu, E., & Gat, J. R. , 1979, Recycling of Water in the Amazon Basin: An Isotopic Study: Water Resources Research, v.15, no. 5, p. 1250-1258, doi:0043-1397 /79/009 W-0552501.00.

Saunaluoma, S., & Schaan, D. , 2012, Monumentality in Western Amazonian formative societies: geometric ditched enclosures in the Brazilian state of Acre: Antiqua, v.2 no.1 doi:10.4081/antiqua.2012.e1.

Saunaluoma, S., Moat, J., Pugliese, F., & Neves, E. , 2021, Patterned Villagescapes and Road Networks in Ancient Southwestern Amazonia: Latin American Antiquity, v.32, p. 173-187, doi:doi:10.1017/laq.2020.79.

Scholz, D., Mühlinghaus, C., & Mangini, A. , 2009, Modelling d^{13}C and d^{18}O in the solution layer on stalagmite surfaces: Geochimica et Cosmochimica Acta, v.73, p. 2592–2602 doi:10.1016/j.gca.2009.02.015.

Schulz, M., & Mudelsee, M. , 2002, REDFIT: estimating red-noise spectra directly from unevenly spaced paleoclimatic time series: Computers & Geosciences, v. 28, p. 421–426, doi:10.1016/S0098-3004(01)00044-9.

Sigl, M, et al, 2015, Timing and climate forcing of volcanic eruptions for the past 2,500 years: Nature, v. 523, p. 543–549, doi:10.1038/nature14565.

Silva, G., Drumond, A., & Ambrizzi, T. , 2011, The impact of El Niño on South American summer climate during different phases of the Pacific Decadal Oscillation: Theoretical and Applied Climatology, v. 106, p. 307–319, doi:10.1007/s00704-011-0427-7.

Silva, L. C., Sternberg, L., Haridasan, M., Hoffmann, W. A., Miralles-Wilhelm, F., & Franco, A. C. , 2008, Expansion of gallery forests into central Brazilian savannas: Global Change Biology, v. 14(9), p. 2108-2118, doi:10.1111/j.1365-2486.2008.01637.x.

Smith, R. J., & Mayle, F. E. , 2018, Impact of mid- to late Holocene precipitation changes on vegetation across lowland tropical South America: a paleo-data synthesis: Quaternary Research, v. 89, no. 1, p. 134-155, doi:10.1017/qua.2017.89.

Souza, J. G. et al, 2019, Climate change and cultural resilience in late pre-Columbian Amazonia: Nature Ecology and Evolution, v. 3, p. 1007–1017, doi:10.1038/s41559-019-0924-0.

Souza, P., & Cavalcanti, I. F. , 2009, Atmospheric centres of action associated with the Atlantic ITCZ position: Inernational Journal of Climatology, v. 29, p. 2091-2105, doi:10.1002/joc.

Taylor, Z. P., Horn, S. P., Mora, C. I., Orvis, K. H., & Cooper, L. W, 2010, A multi-proxy paloecological record of late-Holocene forest expansion in lowland Bolivia: Paleogeogr. Paleoclimatol. Paleoecol., v. 293, p. 98-107, doi:10.1016/j.paleo.2010.05.004.

Thompson, L. G., Mosley-Thompson, E., Davis, M. E., Zagorodnov, V. S., Howat, I. M., Mikhalenko, V. N., & Lin, P.-N, 2013, Annually Resolved Ice Core Records of Tropical Climate Variability over the Past ~1800 Years: Science, v. 340(6135), p. 945-950, doi:10.1126/science.1234210.

Trouet, V., Esper, J., Graham, N. E., Baker, A., Scourse, J. D., & Frank, D. C. , 2009, Persistent Positive North Atlantic Oscillation Mode Dominated the Medieval Climate Anomaly: Science, v. 324, p. 78-80, doi:10.1126/science.1166349.

Utida, G, et al, 2020, Climate changes in Northeastern Brazil from deglacial to Meghalayan periods and related environmental impacts: Quaternary Science Reviews, v. 250, p. 106655, doi:10.1016/j.quascirev.2020.106655.

Van Breukelen, M. R., Vonhof, H. B., Hellstrom, J. C., Wester, W. C., & Wester, W. C., 2008, Fossil dripwater in stalagmites reveals Holocene temperature and rainfall variation in Amazonia: Earth and Planetary Science Letters, v. 275, p. 54-60, doi:10.1016/j.epsl.2008.07.060.

Vera, C, et al, 2006, The South American low-level jet experiment: Bulletin of the American Meteorological Society, v. 87, no. 1, p. 63-77, doi:10.1175/BAMS-87-1-63.

Vuille, M, 2012, A review of the South American monsoon history as recorded in stable isotopic proxies over the past two millennia: Climate of the Past, v. 8, no. 4, p. 1309-1321, doi:10.5194/cp-8-1309-2012.

Wang, X, et al, 2017, Hydroclimate changes across the Amazon lowlands over the past 45,000 years: Nature, v.541, no. 7636,p. 204-207, doi:10.1038/nature20787.

Watling, J. et al, 2017, Impact of pre-Columbian “geoglyph” builders on Amazonian forests: Proceedings of the National Academy of Sciences, v. 114, p. 1868-187, doi:10.1073/pnas.1614359114.

Werth, D., & Avissar, R. , 2002, The local and global effects of Amazon deforestation David: Journal of Geophysical Research, v. 107, p. 55.1-55.8.

Zilli, M. T., Carvalho, L. M., & Lintner, B. R. , 2019, The poleward shift of South Atlantic Convergence Zone in recent decades: Climate Dynamics, v. 52, no. 5-6, p. 2545-2563, doi:10.1007/s00382-018-4277-1.

APPENDEX I – U/Th dates

^{230}Th dating results. The error is 2s error.

Sample Number	**^{238}U (ppb)**	**^{232}Th (ppt)**	**^{230}Th / ^{232}Th (atomic x10^{-6})**	**d^{234}U* (measured)**	**^{230}Th / ^{238}U (activity)**	**^{230}Th Age (yr) (uncorrected)**	**^{230}Th Age (yr) (corrected)**	**d^{234}U$_{\text{Initial}}$** (corrected)**	**^{230}Th Age (yr (corrected)**	**Years C.E.**
PIM-04-2	5209.2 ±13.1	954 ±20	43 ±4	1288.1 ±3.3	0.0005 ±0.0000	23 ±2	**20 ±3**	1288 ±3	**-47 ±3**	1997
PIM-4-9	6075.6 ±7.8	1207 ±24	137.9 ±4.2	1281 ±2.5	16.614 ±0.00004	79 ±2	**77 ±3**	1281.3 ±2.5	**7 ±3**	1943
PIM4-12	5468.9 ±19.1	2058 ±42	121 ±3	1288.4 ±3.5	0.0028 ±0.0000	131 ±2	**126 ±4**	1289 ±3	**58 ±4**	1892
PIM-4-19	4938.5 ±6.2	2617 ±53	144.4 ±3.4	1291 ±2.7	46.402 ±0.00006	221 ±3	**214 ±6**	1291.8 ±2.7	**144 ±6**	1806
PIM-04-21.1	5595.7 ±15.9	1100 ±22	394 ±9	1277.9 ±3.3	0.0047 ±0.0000	225 ±2	**223 ±3**	1279 ±3	**156 ±3**	1794
PIM4-24	5828.9 ±28.8	29077 ±602	31 ±1	1306.8 ±5.6	0.0094 ±0.0001	447 ±3	**384 ±45**	1308 ±6	**314 ±45**	1636
PIM-4-25	5999.4 ±7.2	6861 ±138	156.9 ±3.3	1313.9 ±2.3	108.828 ±0.00006	514 ±3	**499 ±11**	1315.7 ±2.3	**429 ±11**	1521
PIM4-27	5541.6 ±18.0	8189 ±166	146 ±3	1328.9 ±3.5	0.0131 ±0.0001	613 ±3	**594 ±13**	1331 ±3	**526 ±13**	1424
PIM-4-36	5576 ±4.8	8099 ±162	165.5 ±3.4	1308.9 ±1.8	145.767 ±0.00005	690 ±3	**672 ±13**	1311.4 ±1.8	**602 ±13**	1348
PIM-04-41	4972.1 ±9.4	1604 ±33	810 ±17	1320.0 ±2.4	0.0158 ±0.0001	747 ±5	**743 ±5**	1323 ±2	**676 ±5**	1274
PIM4-46	6509.9 ±20.5	5102 ±103	365 ±7	1311.3 ±3.2	0.0174 ±0.0001	822 ±3	**812 ±8**	1314 ±3	**744 ±8**	1206
PIM-04-51	5371.0 ±10.2	378 ±8	4314 ±96	1308.2 ±2.4	0.0184 ±0.0001	872 ±3	**871 ±3**	1311 ±2	**804 ±3**	1146
PIM4-54	3577.7 ±9.6	3843 ±78	323 ±7	1331.6 ±3.3	0.0210 ±0.0001	987 ±4	**974 ±10**	1335 ±3	**904 ±10**	1046
PIM4-59	3981.1 ±12.4	9035 ±183	186 ±4	1314.8 ±3.5	0.0256 ±0.0001	1211 ±5	**1183 ±21**	1319 ±4	**1115 ±21**	835
PIM4-65	3734.5 ±6.3	738 ±15	2264 ±46	1314.7 ±2.3	0.0271 ±0.0001	1284 ±4	**1281 ±4**	1319 ±2	**1211 ±4**	739
PIM-04-69	4051.9 ±7.8	546 ±12	3429 ±74	1307.5 ±2.6	0.0280 ±0.0001	1330 ±6	**1328 ±7**	1312 ±3	**1261 ±7**	689
PIM4-77	5456.9 ±13.2	546 ±11	4941 ±101	1327.1 ±3.1	0.0300 ±0.0001	1411 ±4	**1410 ±5**	1332 ±3	**1340 ±5**	610
PIM-04-87	4977.7 ±9.6	785 ±16	3315 ±69	1347.7 ±2.6	0.0317 ±0.0001	1480 ±5	**1478 ±5**	1353 ±3	**1411 ±5**	539
PIM4-91	4272.0 ±9.0	3156 ±64	738 ±15	1354.1 ±2.8	0.0331 ±0.0001	1540 ±5	**1531 ±8**	1360 ±3	**1461 ±8**	489
PIM4-102	5367.4 ±12.7	145 ±3	20876 ±462	1356.5 ±2.9	0.0341 ±0.0001	1588 ±5	**1588 ±5**	1363 ±3	**1518 ±5**	432
PIM4-115	6196.9 ±16.1	276 ±6	13201 ±277	1356.6 ±3.1	0.0356 ±0.0001	1659 ±5	**1658 ±5**	1363 ±3	**1588 ±5**	362
PIM-05-6	6610.1 ±17.0	2286 ±46	1530 ±31	1425.0 ±3.2	0.0321 ±0.0001	1451 ±6	**1447 ±7**	1431 ±3	**1380 ±7**	570
PIM5-207	6905.2 ±19.5	1799 ±36	2150 ±44	1421.5 ±3.1	0.0340 ±0.0001	1538 ±5	**1535 ±6**	1428 ±3	**1465 ±6**	485
PIM-05-7	6529.5 ±16.8	3300 ±67	1189 ±24	1442.6 ±3.2	0.0364 ±0.0001	1637 ±6	**1631 ±7**	1449 ±3	**1564 ±7**	386
PIM-05-8	4688.7 ±7.7	3393 ±69	866 ±18	1414.4 ±2.5	0.0380 ±0.0002	1729 ±9	**1720 ±11**	1421 ±2	**1653 ±11**	297
PIM-05-9	7226 ±21.3	4169 ±84	1166 ±24	1434.6 ±3.4	0.0408 ±0.00015	1840 ±7	**1833 ±9**	1442.0 ±3.4	**1766 ±9**	184
PIM5-294	7763.7 ±19.5	8218 ±166	661 ±13	1430.3 ±3.0	0.0424 ±0.0001	1917 ±6	**1904 ±11**	1438 ±3	**1834 ±11**	116
PIM5-311	12608.0 ±53.3	15678 ±322	593 ±12	1417.4 ±4.0	0.0447 ±0.0002	2032 ±11	**2017 ±15**	1426 ±4	**1947 ±15**	3
PIM-05-10	5912.1 ±13.6	5429 ±110	813.4 ±16.6	1430.3 ±3.2	0.0453 ±0.00018	2048 ±8	**2037 ±11**	1438.5 ±3.2	**1970 ± 11**	-20
PIM5-339	5813.0 ±24.9	23276 ±478	204 ±4	1414.8 ±4.2	0.0494 ±0.0002	2251 ±11	**2203 ±36**	1424 ±4	**2133 ±36**	-183
PIM5 10.1	6124.0 ±46.3	6948 ±156	703.6 ±16.0	1401.5 ±8.5	0.04842 ±0.00041	2217 ±20	**2203 ±22**	1410.2 ±8.6	**2134 ± 22**	-184
PIM-05-11	5498.0 ±13.0	1108 ±23	3984.0 ±82.3	1419.5 ±3.0	0.0487 ±0.00017	2213 ±8	**2211 ±9**	1428.3 ±3.1	**2144 ± 9**	-194
PIM5-379	5318.0 ±23.1	3010 ±62	1513 ±31	1416.0 ±4.3	0.0519 ±0.0003	2365 ±14	**2358 ±14**	1425 ±4	**2288 ±14**	-338
PIM5-413	5103.3 ±20.7	6735 ±138	705 ±14	1445.3 ±4.2	0.0564 ±0.0003	2541 ±12	**2525 ±17**	1456 ±4	**2455 ±17**	-505
PIM-05-12	6586.2 ±16.3	5046 ±102	1247.5 ±25.4	1439.6 ±3.1	0.05797 ±0.00020	2617 ±10	**2608 ±12**	1450.2 ±3.2	**2541 ± 12**	-591
PIM5-479	5249.3 ±27.1	7928 ±165	695 ±15	1404.8 ±5.1	0.0637 ±0.0004	2919 ±19	**2901 ±23**	1416 ±5	**2831 ±23**	-881
PIM-05-14	4549.5 ±10.4	3342 ±67	1454.9 ±29.5	1416.2 ±3.1	0.06482 ±0.00020	2958 ±10	**2949 ±12**	1428.1 ±3.1	**2882 ± 12**	-932

U decay constants: l$_{238}$ = 1.55125x10^{-10} (Jaffey et al., 1971) and l$_{234}$ = 2.82206x10^{-6} (Cheng et al., 2013). Th decay constant: l$_{230}$ = 9.1705x10^{-6} (Cheng et al., 2013).

*d^{234}U = ([^{234}U/^{238}U]$_{\text{activity}}$ – 1)x1000. ** d^{234}U$_{\text{initial}}$ was calculated based on ^{230}Th age (T), i.e., d^{234}U$_{\text{initial}}$ = d^{234}U$_{\text{measured}}$ x e^{l234xT}.

Corrected ^{230}Th ages assume the initial ^{230}Th/^{232}Th atomic ratio of 4.4 ±2.2 x10^{-6}. Those are the values for a material at secular equilibrium, with the bulk earth ^{232}Th/^{238}U value of 3.8. The errors are arbitrarily assumed to be 50%.

***B.P. stands for "Before Present" where the "Present" is defined as the year 1950 A.D.